

FRAGMENTATION AND HISTORY OF COMET PAIR C/1844 Y1 AND C/2019 Y4

ZDENEK SEKANINA

La Canada Flintridge, California 91011, U.S.A.; ZdenSek@gmail.com

Version July 24, 2023

ABSTRACT

I call attention to extraordinary features displayed by the genetically related long-period comet pair of C/1844 Y1 (Great Comet) and C/2019 Y4 (ATLAS). The issue addressed most extensively is the fragmentation and disintegration of the latter object, itself a thousands-of-years-old fragment. Of the four fragments of C/2019 Y4 recognized by the Minor Planet Center — A, B, C, and D — I confirm that B was the principal mass, which stayed undetected until early April. The comet's 2020 fragmentation is proposed to have begun with a separation of B and A near 22 January, when the nuclear condensation suddenly started to brighten rapidly. From late January to early April, only Fragment A was observed. The remaining Fragments C and D split off most probably from A in mid-March, but they too were detected only in April. A new fragment, E, is proposed to have been observed on three days. Further addressed are the issues of the orbital period and antitail of C/1844 Y1 and the extreme position of this pair among the genetically related groups/pairs of long-period comets.

Subject headings: individual comets: C/1844 Y1, C/2019 Y4; methods: data analysis

1. INTRODUCTION

The arrival of comet C/2019 Y4 a few years ago was the most recent addition to the category of pairs or small groupings of common-origin long-period comets, with the members passing perihelion months, years, decades, or even centuries apart. Discovered by Project ATLAS, *Asteroid Terrestrial-Impact Last Alert System*, the 2019 comet was a distant companion to the brilliant comet C/1844 Y1 (Green 2020a), having apparently broken all records by returning to perihelion not until 175.5 yr later. As fragments of a common parent, they are believed to have been its parts until about the time of perihelion passage several thousand years ago. The time span of almost two centuries between the two fragments' arrivals dwarfs those of only 8 to 32 years exhibited by the three companions to C/1988 A1 (Liller), the leading bright member of the best known comet group of this kind. The recent fragment of that group, C/2019 Y1 (ATLAS), was by sheer coincidence discovered by the same project (Green 2020b) only twelve days before C/2019 Y4. In Section 7 I will return to the relationships among the long-period comets' companions in general and between C/1844 Y1 and C/2019 Y4 in particular.

The early recognition by M. Meyer of the near identity between the orbits of C/2019 Y4 and C/1844 Y1 (Green 2020a) was enough to turn the former object into a likely candidate for preperihelion disintegration. It is known that most companions of the split comets have fairly short lifetimes, which statistically vary as an inverse 0.4 power of the nongravitational acceleration (Sekanina 1982). Even though scatter is rather large, for nearly-parabolic comets the lifetime tends to vary as $q^{-\frac{1}{2}}$, and it can be demonstrated that for $q = 0.25$ AU only massive fragments (with a nongravitational acceleration lower than 3 units of 10^{-5} the solar gravitational acceleration, or approximately 10^{-8} AU day $^{-2}$ at heliocentric distance of 1 AU) should survive one full revolution about the Sun. This condition was apparently satisfied by C/1844 Y1, but not by C/2019 Y4.

2. THE LIGHT CURVE OF C/2019 Y4

The monitoring of brightness variations, as the often readily available signature of a comet, is very useful in order to outline and understand its activity even when the object is evolving in a normal, fairly foreseeable fashion; it is absolutely essential when the object is subjected to irregular, explosive processes. For any comet under observation, information on the brightness evolution of the nuclear condensation is customarily provided online by observers alongside the CCD astrometric data in the *Minor Planet Electronic Circulars* (MPEC) and later on in the *Minor Planet Circulars*, both issued by the *Minor Planet Center* (MPC). The total visual or CCD magnitudes are conveniently available online from the *International Comet Quarterly* (ICQ) or the Crni Vrh Observatory's *Comet Observation Database* (COBS).

Comet C/2019 Y4 had been discovered on 28 December 2019, but subsequently a pair of its pre-discovery images was spotted in a *Catalina Sky Survey* field taken on 20 December (e.g., MPC Staff 2020). A set of selected apparent CCD magnitudes of the nucleus condensation reported between 20 December and 25 February 2020 is plotted in Figure 1. Each data point is an average of such magnitudes obtained on a given night at a given observing site. Practically the same curve, with only moderately increased scatter, would result, if all available data were plotted instead.

The remarkable feature of the figure is a sudden change in the slope of the light curve around 22 January. The apparent nuclear brightness, essentially constant before this date, began to rise at an essentially constant rate of about 0.11 mag per day afterwards. This behavior of the light curve is entirely unlike a typical outburst, because the rate of brightening is much too slow and the duration of brightening much too long; instead of a fraction of a day or a few days at most, the brightness was continuing to rise over a period of longer than a month, with no sign of ebbing. I will return to the significance of this phenomenon in Section 3.

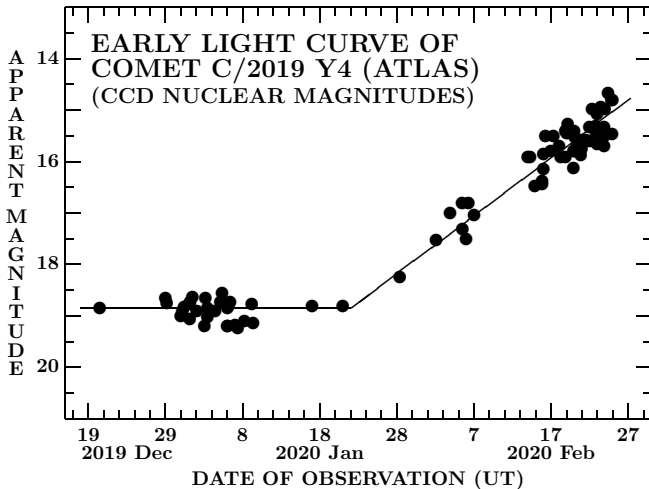


Figure 1. Early light curve of the nuclear condensation of Comet C/2019 Y4 based on a set of selected CCD observations between 20 December 2019 and 25 February 2020. The curve shows no trend until about 22 January, at which time the brightness began to increase exponentially (linearly on the magnitude scale). The data are from MPEC 2020-K131.

By the end of February the comet became bright enough that visual observers could begin to apply their methods of total-brightness determination. Examples of light curves, based on such fairly systematic data sets, as well as on large-aperture CCD imaging, are displayed in Figure 2 from 25 February 2020 on. These light curves were generated independently of the efforts directed towards the comet’s astrometry.

Cursory inspection of the four curves shows both commonalities and differences. They all indicate the comet to have been brightening up to 25–29 March, the peak rates reaching 0.20 ± 0.07 mag per day. The CCD curves show the peak brightness fainter than magnitude 8, whereas the visual curves indicate it was between 7 and 8; this only may mean that the visual observers were accounting for the outer regions of the coma, which were outside the CCD imaging apertures. The brightness decline during April appears to have been very modest and the minimum even broader than the late-March peak. The most complete light curve in Figure 2, by T. Lehmann, shows that in May the comet slowly brightened again, while C. Harder’s results suggest the opposite. The comet was last seen on 21 May, 10 days before perihelion.

3. NUCLEAR FRAGMENTATION OF C/2019 Y4

The earliest indirect evidence of possible splitting of the nucleus was published on 5 April, when S. Nakano reported detection of the sudden appearance of nongravitational perturbations of the comet’s orbital motion (Green 2020c). A day later Ye & Zhang (2020) suggested that the comet may be disintegrating, as images taken on 5 April with a 60-cm telescope of the Xingming Observatory showed an “elongated pseudo-nucleus.” On 7 April a secondary feature was found by E. Guido et al. to be embedded in the tail several arcseconds from the nuclear condensation and then two more features in images taken at the Celado Observatory (Green 2020d). By 13 April CCD images obtained by many observers showed that this comet had unquestionably fragmented.

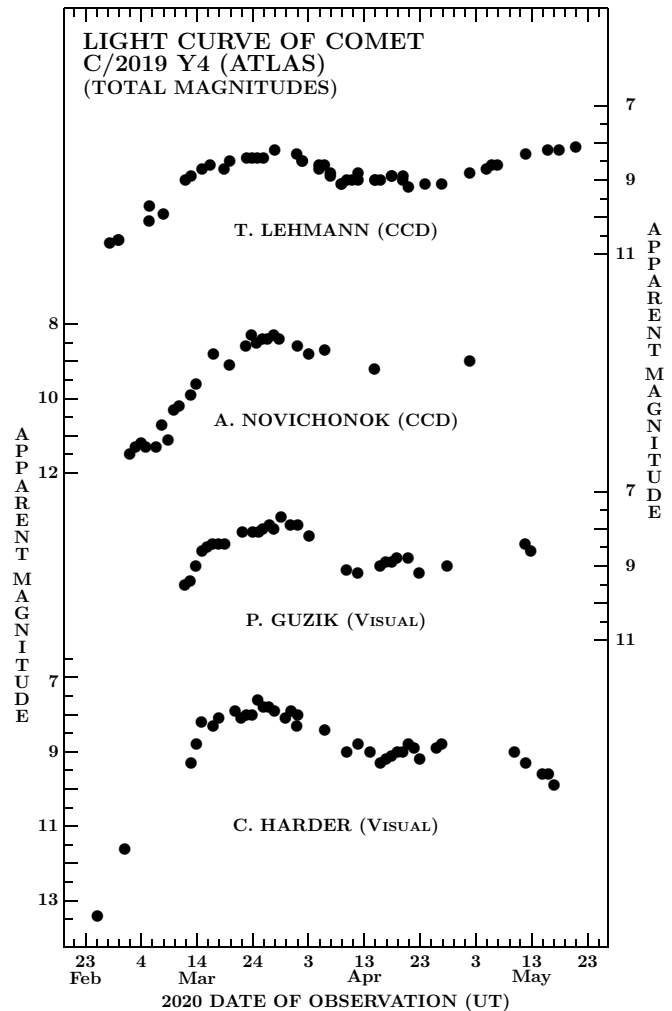


Figure 2. Light curves of Comet C/2019 Y4 (total magnitudes) by two CCD and two visual observers; around 25 February the total brightness is estimated at about 2–3 magnitudes higher than the nuclear brightness in Figure 1. The rate of brightening from that time on, up to late March, is even steeper than the rate exhibited by the data for the nuclear condensation before 25 February.

To examine the time sequence of the nuclear fragmentation of this comet, I adopt the classification of fragments by the MPC Staff (2020), according to which up to four condensations — A, B, C, and D — could be measured from the Earth; Fragment B was proposed as the principal mass. This identity is being confirmed by my dynamical modeling below. The MPC Staff similarly established that the object which had provisionally been designated as Fragment E, was subsequently identified as Fragment B.

Application of the fragmentation model that I introduced nearly 50 years ago (Sekanina 1977) and its expanded version (Sekanina 1978) allow one to obtain multiparametric solutions from sets of separation vectors of any two fragments. Since the astrometric data published for comet C/2019 Y4 are the fragments’ equatorial coordinates (MPC Staff 2020), the relevant input for the proposed modeling is provided by the astrometric positions of fragment pairs at the given times. As the first step, the instances and fragments for which such data are

Table 1

List of Multiple-Fragment Astrometric Observations of C/2019 Y4

Time of observation 2020 (UT)	Obs. code	Nom. frag-ments	Sta-tus	Time of observation 2020 (UT)	Obs. code	Nom. frag-ments	Sta-tus
Apr 6.87924	970	A,B	fix	Apr 11.90035	204	A,C	ok
8.81700	K51	A,C	fix	11.90101	C10	A,B,D	ok
9.80653	K51	B,D	fix	11.90888	C10	A,B,C	fix
9.84611	204	A,C	ok	11.91343	204	A,C	ok
9.85549	970	A,B	fix	11.92651	204	A,C	ok
9.85727	J95	A,B	ok	11.93959	204	A,C	ok
9.85921	204	A,C	ok	13.18954	658	A,B,D	ok
9.87230	970 ^a	A,C	ok	13.19262	658	A,B,D	ok
9.87841	970	A,B	fix	13.19262	658	A,B,D	ok
9.88540	204	A,C	ok	13.19571	658	A,B,D	ok
9.88951	J95	A,B	ok	13.19880	658	A,B,D	ok
10.81943	A77	A,C	fix	13.20189	658	A,B,D	ok
10.82607	A77	A,C	ok	13.86573	J95	A,B,C,D	ok
10.83319	A77	A,C	fix	13.86712	J77	A,B,D	ok
10.84504 ^b	204	B,C	fix	13.88081	J95	A,B,C,D	ok
10.84814	970	A,C	ok	14.86279	970	A,B,D	fix
10.86686	204	A,C	ok	14.87810	970	A,B,D	ok
10.87776	204	A,C	ok	14.88379	J77	A,B	ok
10.88363	J95	A,B	ok	14.90103	J95	A,B,D	ok
10.88647	970	A,C	ok	14.91526	Z80	B,D	fix
10.88683	J77	A,B,C	ok	14.91613	J95	A,B,D	fix
10.92154	J95	A,B	ok	14.91977	Z80	B,D	fix
11.83133	215 ^c	C,D	ok	15.86130	J77	A,B	ok
11.85444	J95	A,B	ok	15.90786	J77	A,B	ok
11.86991	J95	A,B	ok	15.92626	204	A,B	ok
11.87079	970	A,B,C	ok	15.94348	204	A,B	ok
11.87207	B56 ^d	C,D	ok	15.96124	204	A,B	ok
11.87740	C10	A,B,D	ok	16.09437	H45	C,D	fix
11.88527	C10	A,B,D	ok	16.09564	H45	C,D	fix
11.88610	970	A,B,C	ok	16.09746	H45	C,D	fix
11.88748	585 ^e	C,D	ok	16.86351	J77	A,B,D	ok
11.89314	C10	A,B,D	ok	17.24276 ^f	F65	A,C,D	fix
11.89376	970	A,B,C	ok	18.23496	F65	A,D	fix

Notes.

^a Position of Fragment A from code 970, position of Fragment C from code 204.

^b Position of Fragment A provided in MPEC 2020-J16, left out from MPEC 2020-K131.

^c Position of Fragment C from code 215, position of Fragment D from code G23.

^d Position of Fragment C from code B56, position of Fragment D from code Z30.

^e Position of Fragment C from code 585, position of Fragment D from code 938.

^f Position of Fragment C provided in MPEC 2020-J16, left out from MPEC 2020-K131.

available are summarized in Table 1. The columns list the time of observation, the standard observatory code, the fragments assigned to the measured astrometric positions by the MPC Staff, and the status, describing the outcome of preliminary tests aimed at finding out which fragments satisfy performed solutions and which do not. The *ok* status acknowledges that the assigned fragments offer consistent results, while the *fix* status warns that revisions are necessary.

The required revisions, presented in Table 2, are re-assigned fragments to the astrometric positions that did not fit the preliminary fragmentation solutions. Such revisions are rather straightforward when only two fragments are involved. In cases of more than two fragments

Table 2

Adopted Corrections in Multiple Fragment Identifications

Time of observation 2020 (UT)	Obs. code	Positions assigned to fragments		
		in MPECs	in this paper	Notes
Apr 6.87924	970	A, B	C, D	
8.81700	K51	A, C	A, D	
9.80653	K51	B, D	A, D?	
9.85549	970	A, B	A, C	
9.87841	970	A, B	A, C	
10.81943	A77	A, C	A, D	
10.83319	A77	A, C	B, C	
10.84504	204	B, C	A, D	1
11.90888	C10	A, B, C	A, B, D	
14.86279	970	A, B, D	A, B?, D	2
14.91526	Z80	B, D	B, C	
14.91613	J95	A, B, D	A, B, C?	
14.91977	Z80	B, D	B, C	
16.09437	H45	C, D	B?, C?	3
16.09564	H45	C, D	B?, C?	3
16.09746	H45	C, D	B?, C?	3
17.24276	F65	A, C, D	A, B, E	4
18.23496	F65	A, D	A?, E	5

Notes.

1. Position of Fragment B is provided in MPEC 2020-J16 but not in MPEC 2020-K131.

2. Position of Fragment B appears to be in error, as offset D–A offers a good fit but offsets A–B and D–B do not.

3. Identification of fragments very uncertain.

4. Position of Fragment B is provided, as that of Fragment C, in MPEC 2020-J16 but not in MPEC 2020-K131. Position assigned in latter Circular to Fragment D appears to refer to a new Fragment E.

5. The pair appears to include a new Fragment E.

the situation could get more confusing. For example, in a configuration of three fragments A, B, and C or D, the third one may better fit as C relative to A, but as D relative to B. Since a fragment cannot be both C and D, a difficult decision has to be made, based for example on the magnitude of the residuals.

In the following I address the relationships among the four fragments. From Tables 1 and 2 it follows that to the terrestrial observers the most extended period of time during which the multiple nucleus can be investigated using the proposed method is 6–18 April, less than two weeks. During this period, the separation distance between Fragments A and B varied rather insignificantly, while Fragments C and especially D were gradually receding from both A and B. Under the circumstances, the most feasible strategy appears to be to investigate first the relation between A and B, and only later the relation of C and D with respect to A and B. Both C and D rapidly grew more diffuse and were obviously disintegrating into expanding clumps of scattered material before the eyes of the observers.

Imaged by the Hubble Space Telescope (HST) on 20 and 23 April, Fragments A and B appeared as clusters of debris as well (Ye et al. 2021). I will not address the HST appearance of the comet in this paper beyond remarking that the considerable degree of fragmentation of the nucleus seen was likely to be due not only to the HST’s superior spatial resolution and detection limit, but also because of the late stage of the rapidly advancing disintegration process.

Table 3
Models for Motion of Fragment A Relative to Fragment B of Comet C/2019 Y4

Parameter/Quantity	Solution BA ₁	Solution BA ₂	Solution BA ₃	Solution BA ₄	Solution BA ₅	Solution BA ₆
Time of separation, $t_s - t_\pi$ (days)	(-130)	(-130)	(-130)	(-75)	(-130)	(-130)
Date of separation (UT)	(2020 Jan 22)	(2020 Jan 22)	(2020 Jan 22)	(2020 Mar 17)	(2020 Jan 22)	(2020 Jan 22)
Heliocentric distance (AU)	(2.59)	(2.59)	(2.59)	(1.74)	(2.59)	(2.59)
Acceleration (10^{-5} solar gravity)	21.7 ± 2.8	32 ± 20	85 ± 10	2.52 ± 0.80	-10.28 ± 0.79
Separation velocity (m s^{-1})	1.84 ± 0.15	1.65 ± 0.96	3.06 ± 0.25	4.64 ± 0.29	0.78 ± 0.05
Radial component (m s^{-1})	-0.76 ± 1.51	$+1.62 \pm 0.22$
Transverse component (m s^{-1})	-0.32 ± 0.05	-0.28 ± 0.10	-0.40 ± 0.06	-0.99 ± 0.12
Normal component (m s^{-1})	$+1.81 \pm 0.15$	$+1.44 \pm 0.75$	$+2.56 \pm 0.26$	$+4.53 \pm 0.30$	$+0.78 \pm 0.05$
Mean residual	$\pm 0''.52$	$\pm 0''.53$	$\pm 0''.53$	$\pm 0''.55$	$\pm 0''.69$	$\pm 1''.66$
Number of observations	33	33	33	33	33	33

Note.

t_π is the perihelion time. Solutions are presented in the order of increasing mean residual. Assumed separation times are parenthesized, an acceleration or separation velocity components assumed to be zero are dotted. A positive acceleration value means that B is the principal mass, a negative acceleration value means that it is A. The distributions of residuals from Solutions BA₄, BA₅ and BA₆ show minor (up to $0''.5$), distinct (up to at least $1''$), and considerable (up to $3''$) systematic trends, respectively.

The model applied in the following is described in detail in Sekanina (1977, 1978) and its features are summarized in Sekanina (1982). Here I only note that the model allows one to determine up to five parameters: the time of separation, the nongravitational acceleration (actually the companion, or secondary mass, is always *decelerated* relative to the principal mass), and, if needed, the three components (radial, transverse, and normal) of the separation velocity of the companion from the principal mass. The acceleration’s variation with heliocentric distance is approximated by an inverse square power law and the magnitude is usually expressed in units of 10^{-5} the solar gravitational acceleration. In practice, the parameters are determined by a least-squares differential-correction optimization procedure, but the user is allowed to attach any value(s) to any one or more of the five parameters and circumvent its optimization if he chooses to do so (or has to in order to maintain the convergence). This is an extremely useful feature, which implies that the model is effectively provided in 31 different versions.

The optimized differential nongravitational acceleration as the model’s primary driver for separating fragments is linked to another important feature: its sign automatically determines which of the two tested fragments, X or Y, is the principal one. It makes no difference whether one tests a set of separation vectors Y–X or X–Y. If a model solution derived from the Y–X set yields a positive acceleration, X is the principal fragment and vice versa. Similarly with the set X–Y.

3.1. Fragments A and B

Inspection of the employed data, reported by the MPC and summarized in Table 1, indicates that Fragments A and B were simultaneously imaged 38 times in the period of 6–18 April, but the results of preliminary tests presented in Table 2 suggest that on a few occasions at least one of the two fragments was either misidentified or its position measured too inaccurately to be of any use in the model computations. Adopting a rejection cutoff of $\pm 1''.5$ for the residuals $O - C$ (observed minus computed from the model) of A–B in right ascension and declination, the number of acceptable observations has turned out to equal 33.

My efforts were first directed toward the simplest, two-parameter solution, trying to determine the time of separation of Fragment A from Fragment B and the nongravitational acceleration of A relative to B. I began with a separation time of 75 days before perihelion, based on Hui & Ye’s (2020) conclusion that “the comet has disintegrated since 2020 mid-March.” Unfortunately, after a few initial iterations suggesting a meaningless separation time as far back in time as some 600 days (sic) before perihelion, the differential-correction optimization procedure failed to converge. Similarly disappointing were the successive attempts at solutions with more than two parameters.

The overall impression from these runs was that even though the separation time appeared to be indeterminate, the solutions in which the separation was *assumed* to have taken place much earlier than ~ 100 days before perihelion (say, prior to February 2020) looked distinctly preferable, offering a lower mean residual and better distribution of individual residuals.

Given that splitting of a comet’s nucleus is known to often coincide with suddenly elevated activity showing up as a brightening in the light curve, the abrupt change in the slope around 22 January, or 130 days before perihelion, in Figure 1 is a strong suspect as a potential candidate for the fragmentation event that gave birth to components A and B. Incorporating this assumption, the one-parameter solution fitted the observations with an unacceptably high mean residual and with the individual residuals displaying strong systematic trends of up to some $3''$. Solving in addition for the normal component of the separation velocity improved the solution’s quality (BA₅ in Table 3), the systematic trends in the distribution of residuals now reaching not more than about $1''$.

The most satisfactory fit to the data was offered by a three-parameter solution, presented in Table 3 as BA₁. The acceleration slightly exceeds 20 units of 10^{-5} the solar gravitational acceleration and the separation velocity stays below 2 m s^{-1} . The table shows that this solution is distinctly preferable to BA₄, an equivalent solution for an *assumed* separation time of 75 days before perihelion (mid-March), which requires a high separation velocity of nearly 5 m s^{-1} and an acceleration of companion A that

Table 4
Separations of Fragment A from Fragment B of C/2019 Y4
and Residuals from Solution BA₁ (Equinox J2000)

Time of observation 2020 (UT)	Separation A–B		Residual ^a O–C		Obs. code
	in R.A.	in Decl.	in R.A.	in Decl.	
Apr 6.87924	–1′.1	+0′.5	(+4′.0	–2′.0)	970
9.85549	–9.5	+1.9	(–5.0	–0.4)	970
9.85727	–5.0	+2.1	–0.5	–0.2	J95
9.87841	–7.7	+2.9	(–3.2	+0.6)	970
9.88951	–4.8	+2.8	–0.3	+0.5	J95
10.88363	–4.1	+2.1	+0.2	–0.2	J95
10.88683	–3.9	+2.7	+0.4	+0.4	J77
10.92154	–4.6	+2.1	–0.3	–0.2	J95
11.85444	–3.4	+2.6	+0.7	+0.3	J95
11.86991	–4.6	+2.1	–0.6	–0.2	J95
11.87079	–3.1	+2.6	+0.9	+0.3	970
11.87740	–4.5	+2.3	–0.5	0.0	C10
11.88527	–3.2	+2.4	+0.8	+0.1	C10
11.88610	–3.1	+1.9	+0.9	–0.4	970
11.89314	–4.1	+1.5	–0.1	–0.8	C10
11.89376	–4.1	+2.2	–0.1	–0.1	970
11.90101	–4.3	+2.4	–0.3	+0.1	C10
11.90888	–5.3	+1.4	–1.3	–0.9	C10
13.18954	–4.4	+2.2	–0.7	–0.1	658
13.19262	–3.7	+2.9	0.0	+0.6	658
13.19571	–3.3	+4.0	(+0.4	+1.7)	658
13.19880	–3.7	+3.3	0.0	+1.0	658
13.20189	–4.7	+2.9	–1.1	+0.6	658
13.86573	–3.1	+2.8	+0.4	+0.4	J95
13.86712	–3.3	+2.8	+0.2	+0.4	J77
13.88081	–3.1	+2.5	+0.4	+0.1	J95
14.86279	–1.9	+0.7	(+1.3	–1.7)	970
14.87810	–3.0	+1.5	+0.1	–0.9	970
14.88379	–3.0	+3.3	+0.2	+0.9	J77
14.90103	–2.6	+2.1	+0.6	–0.3	J95
14.91613	–2.0	+2.5	+1.2	+0.1	J95
15.86130	–3.6	+2.5	–0.7	0.0	J77
15.90786	–3.1	+2.6	–0.3	+0.1	J77
15.92626	–2.6	+2.2	+0.3	–0.3	204
15.94348	–2.7	+2.1	+0.2	–0.4	204
15.96124	–2.7	+2.1	+0.1	–0.4	204
16.86351	–3.1	+2.1	–0.5	–0.5	J77
17.24276 ^b	–2.7	+2.7	–0.3	0.0	F65

Notes.

^a Entries whose residuals are parenthesized have been excluded from the solution.

^b Position used for Fragment B has been assigned to Fragment C in MPEC 2020-J16 and left out of MPEC 2020-K131.

is four times higher. Solution BA₁ is also preferable to BA₃, in which the contribution from the acceleration is taken over by the (increased) separation velocity. On the other hand, a four-parameter solution BA₂ that incorporates the radial component of the separation velocity among the parameters is a case of overkill, documented by their unacceptably high errors.

The residuals from the fit of Solution BA₁ of Table 3 to the 38 A–B separations in right ascension and declination are listed in Table 4; of the five rejected data points three are incorrect identities (Table 2) and two are inaccurate data. The peculiar separation trajectory of Fragment A relative to B, plotted in Figure 3, is consistent with a scenario that incorporates the fragmentation event in late January and is, in addition, supported by the nuclear-condensation’s light curve in Figure 1 and by the fact

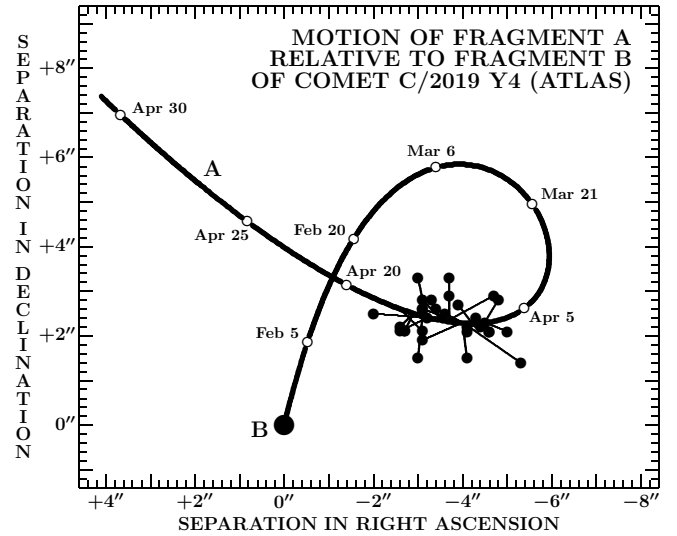


Figure 3. Separation trajectory of Fragment A relative to Fragment B derived from Solution BA₁ in Table 3. The solid circles are the observations of A from Table 4, while the open circles are ephemeris positions (at 0 TT) from the model. The two fragments are assumed to have separated from each other on 22 January 2020, 130 days before perihelion. Note that the nucleus was not seen double during March, even though the separation distance between A and B was greater than in April.

that the nucleus was not seen double during February and especially in March 2020, when the predicted separation distance between the two fragments was much greater than in April (Figure 3).

The key to understanding both the light curve and the detection anomaly is the fundamentally different behavior of the two fragments: while Fragment A was subjected to a high rate of mass loss, *Fragment B* was of low activity and *too faint to detect* in any telescope employed in the comet’s observations. The observed light curve between late January and early April was exclusively a product of Fragment A.

Closer inspection of the light curve shows that the constant apparent brightness of the nuclear condensation between late December 2019 and late January 2020 actually meant a decline of activity. If interpreted in terms of the cross-sectional area of dust grains near the nucleus, the drop was from 96 km² on 20 December to 33 km² on 22 January at an assumed geometric albedo of 4 percent and accounting for the phase effect using the Marcus (2007) law. The observed brightness increase from apparent magnitude of 18.8 on 22 January to 15.0 on 25 February, at a fairly constant rate of 0.11 mag per day is equivalent to an *exponentially* growing cross-sectional area of released dust between the two dates from 33 km² to 367 km². At time t this cross-sectional area equals

$$\mathcal{A}(t) = \mathcal{A}(t_{\text{frg}}) \exp[\zeta(t - t_{\text{frg}})], \quad (1)$$

where t_{frg} is the presumed fragmentation time, 22 January. As $\exp(34\zeta) = 367/33 = 11.1$, one finds $\zeta = 0.071$ per day. The comet brightening continuously at the observed rate of 0.11 mag per day and its description via Equation (1) is thus readily interpreted as progressive disintegration of Fragment A, whose cross-sectional area doubled in approximately 10 days.

Table 5
Models for Motion of Fragment C Relative to Fragments B and A of Comet C/2019 Y4

Parameter/Quantity	Solutions for C relative to B		Solutions for C relative to A	
	Solution BC ₁	Solution BC ₂	Solution AC ₁	Solution AC ₂
Time of separation, $t_s - t_\pi$ (days)	-73.5 ± 4.2	-70.1 ± 4.6	-151 ± 10	-71.2 ± 2.8
Date of separation (UT)	2020 Mar 18.5	2020 Mar 21.9	2020 Jan 1	2020 Mar 20.8
Heliocentric distance (AU)	1.71	1.65	2.88	1.67
Acceleration (10^{-5} solar gravity)	144 ± 37	172 ± 51	24.4 ± 3.2	161 ± 30
Normal separation velocity (m s^{-1})	-0.32 ± 0.38	-2.21 ± 0.41
Mean residual	$\pm 0''.86$	$\pm 0''.87$	$\pm 0''.67$	$\pm 0''.64$
Number of observations	11	11	20	22

Note.

t_π is the perihelion time. Solutions are presented in the order of increasing number of parameters that were solved for. Normal separation velocities assumed to be zero are dotted. No solutions involving transverse and/or radial separation velocity components offered sets of meaningful parameters.

To properly investigate the crumbling of Fragment A that presumably began on 22 January, one should disregard the presence of dust in the atmosphere at that time and \mathcal{A}_{frg} in Equation (1) should be the cross-sectional area of the surface of Fragment A. The value of ζ would then be somewhat higher. For example, taking conservatively the diameter of Fragment A at the time of separation from Fragment B to be 500 meters, one would obtain $\exp(34\zeta) = 4 \times 367 / (\pi \times 0.5^2) \simeq 1870$ or $\zeta = 0.22$ and the doubling time a little over 3 days. For a fragment 100 meters across, $\zeta = 0.32$ and the doubling time more than 2 days.

Continuing with this line of argumentation, let at time $t > t_{\text{frg}}$ the number of pieces of debris of the crumbling fragment be $\mathcal{N}(t)$ and the mean cross-sectional area of one piece $\langle \mathcal{A} \rangle$, so that

$$\langle \mathcal{A} \rangle \mathcal{N}(t) = \mathcal{A}(t) = \mathcal{A}(t_{\text{frg}}) \eta(t), \quad (2)$$

where $\eta(t) = \exp[\zeta(t - t_{\text{frg}})]$. Expressing a cross-sectional area in terms of a characteristic dimension $\mathfrak{R}(t)$, such as the radius or diameter, one can write the conditions for the mean cross-sectional area and volume at time t :

$$\begin{aligned} \langle \mathfrak{R}^2 \rangle \mathcal{N} &= \mathfrak{R}_{\text{frg}}^2 \eta(t), \\ \langle \mathfrak{R}^3 \rangle \mathcal{N} &= \mathfrak{R}_{\text{frg}}^3, \end{aligned} \quad (3)$$

where $\mathfrak{R}_{\text{frg}}^2$ and $\mathfrak{R}_{\text{frg}}^3$ refer to Fragment A at the fragmentation time. The ratio,

$$\frac{\langle \mathfrak{R}^3 \rangle}{\langle \mathfrak{R}^2 \rangle} = \frac{\mathfrak{R}_{\text{frg}}}{\eta(t)}, \quad (4)$$

is a function of the size distribution, $f(\mathfrak{R}) d\mathfrak{R} \sim \mathfrak{R}^{-s} d\mathfrak{R}$, of the debris. If the minimum and maximum dimensions at time t are $\mathfrak{R}_{\text{min}}(t)$ and $\mathfrak{R}_{\text{max}}(t)$, respectively, the mean values are given by

$$\langle \mathfrak{R}^\nu \rangle \int_{\mathfrak{R}_{\text{min}}}^{\mathfrak{R}_{\text{max}}} \mathfrak{R}^{-s} d\mathfrak{R} = \int_{\mathfrak{R}_{\text{min}}}^{\mathfrak{R}_{\text{max}}} \mathfrak{R}^{\nu-s} d\mathfrak{R} \quad (\nu = 2, 3). \quad (5)$$

For less steep distributions, for which $s < 3$ the mean values are essentially independent of $\mathfrak{R}_{\text{min}}$ and the ratio is at time t

$$\frac{\langle \mathfrak{R}^3 \rangle}{\langle \mathfrak{R}^2 \rangle} = \frac{3-s}{4-s} \mathfrak{R}_{\text{max}}(t). \quad (6)$$

Comparison of Equations (4) and (6) gives for the dimension of the largest piece of debris of Fragment A at time t in terms of the fragment's dimension at t_{frg} :

$$\mathfrak{R}_{\text{max}}(t) = \frac{4-s}{3-s} \frac{\mathfrak{R}_{\text{frg}}}{\eta(t)} = \frac{4-s}{3-s} \mathfrak{R}_{\text{frg}} \exp[-\zeta(t - t_{\text{frg}})]. \quad (7)$$

Regardless of exact values for ζ and s (if lower than 3), Equation (7) suggests that months after the separation of A from B, the dimensions of the largest remaining piece of A should be orders of magnitude smaller than the initial size. This is contrary to the results that Ye et al. (2021) obtained from their study of the comet's debris with the HST in late April. It appears that the process of disintegration of Fragment A was proceeding in a highly irregular manner. The rate of disintegration may have varied strongly with time and/or the process affected only a fraction of the object. In any case, the presence of major anomalies is implied by the dramatic fluctuations in the size distribution of the debris of Fragment A, as documented by Ye et al.

3.2. Fragment C and Its Parent

The statistics of the split comets with more than two fragments suggest that, as a rule, the secondary nuclei (or companions) have separated from the principal mass (Sekanina 1982). Less often has a second companion split off instead from the first companion, or, more generally, a companion of a later generation from a companion of an earlier generation. Accordingly, one would expect Fragment C of comet ATLAS to separate, like Fragment A, from B. Yet, it is desirable to test both options. An obvious constraint is that Fragment C could *not* have broken off from A *before* A did from B.

Tables 1 and 2 show that the simultaneous astrometric observations of B and C have been less numerous than those of A and C, and both pairs less numerous than the simultaneous astrometry of B and A. Because of these limitations, the rejection cutoff for examining the parent of C was increased from $1''.5$ to $2''.0$. I applied a variety of the fragmentation model's versions and found that unlike in the case of the motion of Fragment A relative to B, the separation time always converged. However, solutions with higher number of parameters than three consistently failed to converge; the two converging ones for either fragmentation scenario are compared in Table 5.

Table 6Separations of Fragment C from Fragment B of C/2019 Y4 and Residuals from Solution BC₁ (Equinox J2000)

Time of observation 2020 (UT)	Separation C–B		Residual ^a O–C		Obs. code
	in R.A.	in Decl.	in R.A.	in Decl.	
Apr 10.83319 ^b	+7".4	–0".8	+0".2	–0".4	A77
10.84504 ^c	+11.0	–2.9	(+3.8	–2.5)	204
10.88683	+6.1	+0.3	–1.1	+0.7	J77
11.87079	+9.2	+0.2	+1.1	+0.4	970
11.88610	+8.5	–0.3	+0.4	–0.1	970
11.89376	+7.4	–0.2	–0.6	0.0	970
13.86573	+8.7	+1.2	–1.2	+0.8	J95
13.88081	+8.7	+0.5	–1.1	+0.1	J95
14.91526 ^d	+11.6	–0.6	+0.7	–1.3	Z80
14.91613 ^d	+13.2	+1.4	(+2.3	+0.7)	J95
14.91977 ^d	+12.5	+0.7	+1.6	0.0	Z80
16.09437 ^e	+9.9	+0.8	(–2.3	–0.4)	H45
16.09564 ^e	+11.4	+0.5	–0.8	–0.7	H45
16.09746 ^e	+13.0	+0.3	+0.8	–0.9	H45

Notes.

^a Entry whose residuals are parenthesized has been excluded from the solution.

^b Position used for Fragment B has been assigned to Fragment A in MPEC 2020-K131.

^c Positions assigned to Fragment B in MPEC 2020-J16 and to C in MPEC 2020-K131 (B missing from the latter Circular) refer in fact to Fragments A and D, respectively, causing unacceptably large residual of C–B.

^d Position used for Fragment C has been assigned to Fragment D in MPEC 2020-K131.

^e Positions used for Fragments B and C have been assigned to Fragments C and D, respectively, in MPEC 2020-K131.

Solutions BC₁ and BC₂ offer similar separation times, which precede the peak of the light curves in Figure 2 by several days, but Solution BC₁ is preferred because the normal component of the separation velocity from Solution BC₂ is poorly determined and therefore an unnecessary parameter. An unexpected problem is a systematic trend in the residuals in declination, which mars *either* solution. For Solution BC₁ this undesirable anomaly is apparent from Table 6 and very obvious from the separation trajectory of Fragment C relative to Fragment B displayed in Figure 4.

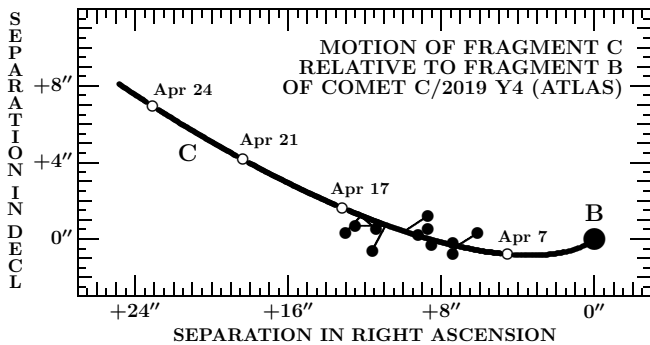


Figure 4. Separation trajectory of Fragment C relative to Fragment B derived from Solution BC₁ in Table 5. The solid circles are the observations of C from Table 6, while the open circles are ephemeris positions (at 0 TT) from the model. Note the systematic trend in the distribution of the data relative to the model curve.

Table 7Separations of Fragment C from Fragment A of C/2019 Y4 and Residuals from Solution AC₂ (Equinox J2000)

Time of observation 2020 (UT)	Separation C–A		Residual ^a O–C		Obs. code
	in R.A.	in Decl.	in R.A.	in Decl.	
Apr 8.81700 ^b	+12".3	–1".2	(+4".0	+1".3)	K51
9.84611	+9.7	–2.2	+0.6	+0.3	204
9.85549	+9.5	–1.9	+0.3	+0.6	970
9.85921	+8.7	–2.1	–0.4	+0.4	204
9.87230	+8.8	–2.8	–0.4	–0.3	970 ^c
9.87841	+7.7	–2.9	–1.5	–0.4	970
9.88540	+8.7	–2.2	–0.5	+0.3	204
10.81943 ^d	+12.0	–4.1	(+1.9	–1.7)	A77
10.82607	+9.6	–2.5	–0.5	–0.1	A77
10.83319 ^e	+7.4	–0.8	(–2.7	+1.6)	A77
10.84814	+9.7	–2.7	–0.4	–0.3	970
10.86686	+9.9	–2.3	–0.2	+0.1	204
10.87776	+10.0	–2.3	–0.1	+0.1	204
10.88647	+10.1	–2.4	0.0	0.0	970
10.88683	+10.0	–2.4	–0.1	0.0	J77
11.87079	+12.3	–2.4	+1.2	–0.2	970
11.88610	+11.6	–2.2	+0.5	0.0	970
11.89376	+11.6	–2.4	+0.4	–0.2	970
11.90035	+12.4	–2.2	+1.2	0.0	204
11.90888 ^b	+13.9	–1.6	(+2.7	+0.6)	C10
11.91343	+12.3	–2.0	+1.1	+0.2	204
11.92651	+12.4	–1.9	+1.2	+0.3	204
11.93959	+11.5	–2.7	+0.2	–0.5	204
13.86573	+11.7	–1.6	–1.6	+0.2	J95
13.88081	+11.8	–2.0	–1.6	–0.2	J95
14.91613 ^f	+15.2	–1.1	+0.6	+0.3	J95

Notes.

^a Entries whose residuals are parenthesized have been excluded from the solution.

^b Position assigned to Fragment C in MPEC 2020-K131 refers in fact to Fragment D, causing unacceptably large residual of C–A.

^c Positions of Fragments A and C observed simultaneously at two codes: A at 970, C at 204.

^d Position assigned to Fragment C in MPEC 2020-K131 refers in fact to Fragment D; even though residual C–A is less than $\pm 2''$ rejection cutoff in either coordinate, strong preference for D is supported by much lower residual D–A.

^e Position assigned to Fragment A in MPEC 2020-K131 refers in fact to Fragment B, causing unacceptably large residual of C–A.

^f Position used for Fragment C has been assigned to Fragment D in MPEC 2020-K131.

Contrary to Solutions BC₁ and BC₂, Solutions AC₁ and AC₂ differ from each other considerably. As seen from both the residuals in Table 7 and from the plot of the separation trajectory in Figure 5, the fit to the data by Solution AC₂ can hardly be better. On the other hand, Solution AC₁ has a number of weaknesses. In the adopted overall fragmentation scenario it is in fact meaningless, because it implies that Fragment C had broken off from Fragment A *before* A separated from B (cf. Section 3.1). In addition, as seen from Table 8, this solution offers acceptable residuals (below 2'') from only 20 of the 22 data points and strong systematic trends of about 1'' are clearly apparent in the distribution of residuals in right ascension.

The presented evidence suggests rather strongly that it is Fragment A that is the parent to Fragment C. The

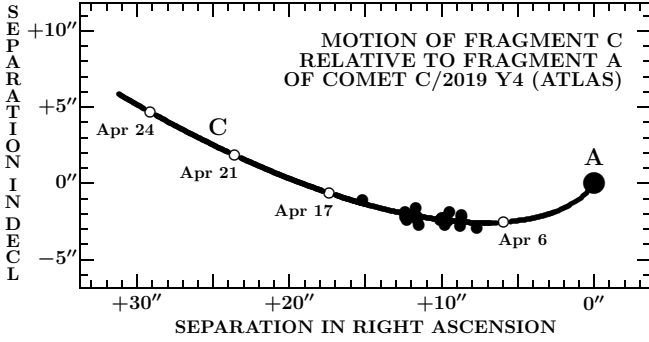


Figure 5. Separation trajectory of Fragment C relative to Fragment A derived from Solution AC₂ in Table 5. The solid circles are the observations of C from Table 7, while the open circles are ephemeris positions (at 0 TT) from the model. Note the excellent agreement between the data and the model, in sharp contrast to the poor fit in Figure 4.

failure to get an acceptable distribution of residuals on the assumption that the parent was the principal mass B obviously had fundamental roots and was not caused by inaccurate astrometric observations.

The determined fragmentation sequence has implications for the meaning of the observed positions of Fragment C relative to Fragment B. Dynamically, their separations represent the sum of separations of C from A and A from B:

$$C-B = (C-A) + (A-B). \quad (8)$$

The averaged daily separations of C–B computed in this fashion for the mean times of observation of this pair (cf. Table 6) are listed in Table 9, where the residuals $O-C$ show rather good accord with the observed separations.

3.3. Fragment D and Its Parent

The examination of the origin and motion of Fragment D has followed closely the routine used in the previous section for Fragment C, including the rejection cutoff of 2''. Unfortunately, the identity of fragments in some observations was somewhat uncertain. Chronologically, the first such case referred to April 10.81943 (code A77), wherein the MPC assigned Fragment C had to be replaced with D. This improved the fit, even though C had been borderline. A more difficult was the observation on April 11.90888 (code C10), likewise requiring that Fragment C be changed to D, mainly because of the poor fit in the C–A separation. Although C–B and D–B fitted reasonably well, C–B had to be rejected. The observation of April 14.86279 (code 970) was a relatively straightforward case; the position of Fragment B apparently was in error, as the separation D–A fitted well, but A–B and D–B did not at all. On the other hand, the observation of April 14.91613 (code J95) was a major conundrum. The separations C–A and D–A pointed to the need to correct the MPC assigned Fragment D to C, as C–A fitted well but D–A did not. But when I tested the separations C–B and D–B, C was a problem. The separation A–B was acceptable, so it was not clear where the culprit was. Fragment C appeared preferable to D, but the contradiction persisted. The final case was the observation of April 14.91977 (code Z80), where I also replaced Fragment D with C, as the separation C–B offered a better fit than D–B, even though both were acceptable.

Table 8
Separations of Fragment C from Fragment A of C/2019 Y4 and Residuals from Solution AC₁ (Equinox J2000)

	Time of observation 2020 (UT)	Separation C–A		Residual ^a $O-C$		Obs. code
		in R.A.	in Decl.	in R.A.	in Decl.	
Apr	9.84611	+9 ^h 7	–2 ^m 2	–0 ^s 2	+0 ^s 4	204
	9.85549	+9.5	–1.9	–0.4	+0.7	970
	9.85921	+8.7	–2.1	–1.2	+0.5	204
	9.87230	+8.8	–2.8	–1.1	–0.2	970 ^b
	9.87841	+7.7	–2.9	(–2.2)	(–0.3)	970
	9.88540	+8.7	–2.2	–1.2	+0.4	204
	10.82607	+9.6	–2.5	–0.8	–0.2	A77
	10.84814	+9.7	–2.7	–0.7	–0.4	970
	10.86686	+9.9	–2.3	–0.5	0.0	204
	10.87776	+10.0	–2.3	–0.4	0.0	204
	10.88647	+10.1	–2.4	–0.3	–0.1	970
	10.88683	+10.0	–2.4	–0.4	–0.1	J77
	11.87079	+12.3	–2.4	+1.4	–0.3	970
	11.88610	+11.6	–2.2	+0.7	–0.1	970
	11.89376	+11.6	–2.4	+0.6	–0.3	970
	11.90035	+12.4	–2.2	+1.4	–0.1	204
	11.91343	+12.3	–2.0	+1.3	+0.1	204
	11.92651	+12.4	–1.9	+1.4	+0.2	204
	11.93959	+11.5	–2.7	+0.5	–0.6	204
	13.86573	+11.7	–1.6	–0.3	–0.1	J95
	13.88081	+11.8	–2.0	–0.2	–0.5	J95
	14.91613	+15.2	–1.1	(+2.6)	(+0.1)	J95

Notes.

^a Entries whose residuals are parenthesized have been excluded from this solution but left acceptable residuals from Solution AC₂.

^b Positions of Fragments A and C observed simultaneously at two codes: A at 970, C at 204.

The results for Fragment D show similarities with the results for Fragment C, except that the numbers of available (B, D) and (A, D) pairs have now been comparable. The fragmentation models are summarized in Table 10, which suggests — like Table 5 for Fragment C — two similar solutions for the motion of D relative to B and two very different solutions relative to A.

Solution BD₂ again includes a normal component of the separation velocity that is not well determined, so that Solution BD₁ is preferred. Unlike in the case of Solution BC₁, the distribution of residuals offered by Solution BD₁ is rather acceptable, as seen from Table 11 and Figure 6.

Table 9
Daily Averages of Fragment C Separation from B of C/2019 Y4 Computed As (C–A)+(A–B), and Mean Residuals from Observations (Equinox J2000)

Mean time of observation 2020 (UT)	Computed C–B		Residual ^a $O-C$		Obs. codes
	in R.A.	in Decl.	in R.A.	in Decl.	
Apr 10.860	+5 ^h 9	–0 ^m 1	+0 ^s 9	–0 ^s 2	A77, J77
11.884	+7.2	+0.1	+1.2	–0.2	970
13.873	+9.9	+0.6	–1.2	+0.3	J95
14.917	+11.5	+1.0	+0.9	–0.5	Z80, J95
16.096	+13.3	+1.5	–1.9	–1.0	H45

Note.

^a Observed minus computed as (C–A)+(A–B).

Table 10
Models for Motion of Fragment D Relative to Fragments B and A of Comet C/2019 Y4

Parameter/Quantity	Solutions for D relative to B		Solutions for D relative to A	
	Solution BD ₁	Solution BD ₂	Solution AD ₁	Solution AD ₂
Time of separation, $t_s - t_\pi$ (days)	-67.1 ± 2.0	-68.1 ± 2.9	-137.3 ± 7.4	-75.9 ± 4.2
Date of separation (UT)	2020 Mar 24.9	2020 Mar 23.9	2020 Jan 14.7	2020 Mar 16.1
Heliocentric distance (AU)	1.60	1.62	2.70	1.75
Acceleration (10^{-5} solar gravity)	290 ± 51	271 ± 59	38.3 ± 4.2	159 ± 34
Normal separation velocity (m s^{-1})	$+0.17 \pm 0.28$	-1.73 ± 0.45
Mean residual	$\pm 0''.83$	$\pm 0''.84$	$\pm 0''.72$	$\pm 0''.84$
Number of observations	16	16	17	20

Note.

t_π is the perihelion time. Solutions are presented in the order of increasing number of parameters that were solved for. Normal separation velocities assumed to be zero are dotted. No solutions involving transverse and/or radial separation velocity components offered sets of meaningful parameters.

Of the two solutions for the motion of Fragment D relative to A, Solution AD₁ is inferior to Solution AD₂ in that it has been unable to fit three of the 20 data points within the rejection cutoff. The full data set, represented by Solution AD₂ with a mean residual of $\pm 0''.84$ (Table 10), has been fitted by Solution AD₁ with a mean residual as high as $\pm 0''.99$. However, unlike Solution AC₁, Solution

AD₁ strictly is not meaningless because its separation from Fragment A is found to have taken place within 1σ of the time of separation of A from B. Although the distribution of residuals is not bad, the solution is shown above to be weak and the derived separation time is not realistic, being affected by neglect of the normal component of the separation velocity. On the other hand, Solution AD₂ and the BD solutions are in fairly close agreement in that D split off from its parent in mid-, or the second half of, March.

For comparison with Solution BD₁, the distribution of residuals offered by Solution AD₂ is displayed in Table 12 and the separation trajectory of Fragment D relative to A is plotted in Figure 7. The plot indicates that except for three data points at the very beginning of the observed segment of the trajectory, the fit is in fact better than the fit to the motion of Fragment D relative to B exhibited in Figure 6.

The other point to argue is that it is unlikely that both fragments, A and B, should have broken up almost simultaneously, one releasing C, the other D. On the other hand, it should not be surprising that the gradually disintegrating A produced, next to the debris, two subfragments in a row, or perhaps one that almost immediately split into two. In any case, there is some evidence for preferring A to B as the parent to D, but it is tenuous.

Table 11

Separations of Fragment D from Fragment B of C/2019 Y4 and Residuals from Solution BD₁ (Equinox J2000)

Time of observation 2020 (UT)	Separation D–B		Residual ^a O–C		Obs. code
	in R.A.	in Decl.	in R.A.	in Decl.	
Apr 9.80653 ^b	+10''.4	–0''.7	(+3''.1	–0''.3)	K51
11.87740	+9.7	–0.1	0.0	–0.2	C10
11.88527	+11.0	0.0	+1.4	–0.1	C10
11.89314	+11.1	–0.8	+1.5	–0.9	C10
11.90101	+9.8	–0.1	+0.1	–0.2	C10
11.90888 ^c	+8.6	–0.2	–1.1	–0.3	C10
13.18954	+9.8	+0.3	–1.7	–0.2	658
13.19262	+10.9	+0.1	–0.6	–0.4	658
13.19571	+11.2	+1.8	–0.2	+1.3	658
13.19880	+10.9	+0.7	–0.6	+0.2	658
13.20189	+10.6	+0.6	–0.9	+0.1	658
13.86573	+12.8	+1.3	+0.4	+0.5	J95
13.86712	+12.2	+1.2	–0.2	+0.4	J77
13.88081	+13.8	+1.0	+1.3	+0.2	J95
14.86279 ^d	+16.0	–0.4	(+2.0	–1.7)	970
14.87810	+14.9	+0.5	+0.9	–0.8	970
14.90103	+14.9	+1.0	+0.8	–0.3	J95
14.91526 ^e	+11.6	–0.6	(–2.5	–1.9)	Z80
14.91613 ^e	+13.2	+1.4	(–0.9	+0.1)	J95
14.91977 ^e	+12.5	+0.7	(–1.6	–0.6)	Z80
16.86351	+16.5	+4.2	–1.0	+1.7	J77

Notes.

^a Entry whose residuals are parenthesized has been excluded from the solution.

^b Position assigned to Fragment B in MPEC 2020-K131 refers instead to Fragment A.

^c Position used for Fragment D has been assigned to Fragment C in MPEC 2020-K131.

^d Position of Fragment B in MPEC 2020-K131 appears to be in error.

^e Position assigned to Fragment D in MPEC 2020-K131 refers instead to Fragment C.

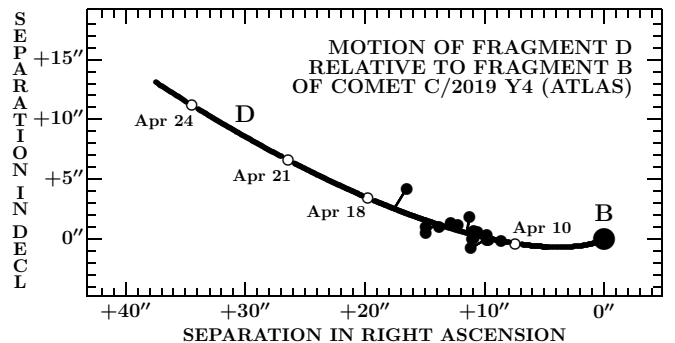


Figure 6. Separation trajectory of Fragment D relative to Fragment B derived from Solution BD₁ in Table 10. The solid circles are the observations of D from Table 11, while the open circles are ephemeris positions (at 0 TT) from the model.

Table 12

Separations of Fragment D from Fragment A of C/2019 Y4 and Residuals from Solution AD₂ (Equinox J2000)

	Time of observation 2020 (UT)	Separation D–A		Residual ^a O–C		Obs. code
		in R.A.	in Decl.	in R.A.	in Decl.	
Apr	8.81700 ^b	+12 ^h :3	–1 ^m :2	+1 ^s :9	+1 ^s :6	K51
	9.80653 ^c	+10.4	–0.7	–1.0	+2.0	K51
	10.81943 ^b	+12.0	–4.1	–0.4	–1.6	A77
	10.84504 ^d	+11.0	–2.9	–1.5	–0.4	204
	11.87740	+14.1	–2.4	+0.5	–0.1	C10
	11.88527	+14.2	–2.4	+0.6	–0.1	C10
	11.89314	+15.3	–2.3	+1.6	0.0	C10
	11.90101	+14.1	–2.5	+0.4	–0.2	C10
	11.90888 ^b	+13.9	–1.6	+0.2	+0.7	C10
	13.18954	+14.2	–1.9	–1.0	0.0	658
	13.19262	+14.5	–2.8	–0.7	–0.9	658
	13.19571	+14.5	–2.2	–0.7	–0.3	658
	13.19880	+14.5	–2.6	–0.7	–0.7	658
	13.20189	+15.3	–2.3	+0.1	–0.4	658
	13.86573	+15.9	–1.5	–0.2	+0.2	J95
	13.86712	+15.5	–1.6	–0.6	+0.1	J77
	13.88081	+16.9	–1.5	+0.8	+0.2	J95
	14.86279	+17.9	–1.1	+0.5	+0.2	970
	14.87810	+18.0	–1.0	+0.6	+0.3	970
	14.90103	+17.5	–1.1	+0.1	+0.2	J95
	14.91613 ^e	+15.2	–1.1	(–2.2	+0.1)	J95
	17.24276 ^f	+20.0	+2.6	(–0.8	+2.7)	F65
	18.23496 ^f	+21.8	+4.3	(–0.6	+3.7)	F65

Notes.

^a Entries whose residuals are parenthesized have been excluded from the solution.

^b Position used for Fragment D has been assigned to Fragment C in MPEC 2020-K131.

^c Position used for Fragment A has been assigned to Fragment B in MPEC 2020-K131.

^d Positions used for Fragments A and D have been assigned, respectively, to Fragments B and C in MPEC 2020-K131.

^e Position assigned to Fragment D in MPEC 2020-K131 refers instead to Fragment C, causing unacceptably large residual of D–A.

^f Position assigned to at least one of Fragments A and D in MPEC 2020-K131 appears to refer to a new fragment, causing unacceptably large residual of D–A.

3.4. New Fragment E

As is apparent from Table 12, the separations of (D–A) on April 17.24276 and 18.23496 UT (code F65) left residuals in declination of almost 3^h and 4^h, respectively, from Solution AD₂. On the other hand, the separation of (A–B) left on the 17th an excellent residual in either coordinate from Solution BA₁ (Table 4), indicating that the problem was not with Fragment A. Under these circumstances, one can rule out that the third fragment on the 17th and the second fragment on the 18th were D. Since Fragment C replacing D would have fitted the separation trajectory even worse, the odds were that on the two days one had to do with a new fragment, E.

Furthermore, given that the separation of (D–A) on April 9.80653 UT (code K51) left, from Solution AD₂ in Table 12, a large residual in declination that essentially equaled the rejection cutoff, it is reasonable to suspect that here too the involved fragment may have been E rather than D. Computer runs linking the observations from April 9.8, 17.2, and 18.2 did indeed lead to success-

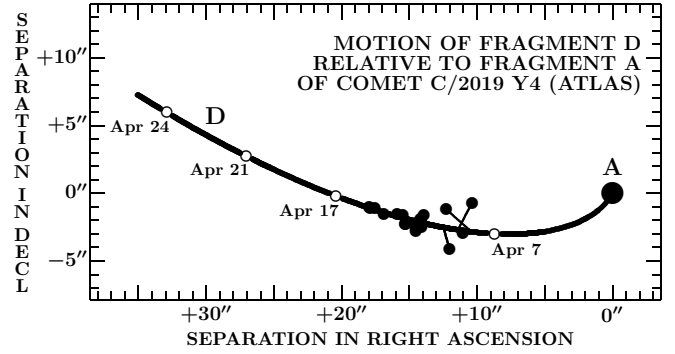


Figure 7. Separation trajectory of Fragment D relative to Fragment A derived from Solution AD₂ in Table 10. The solid circles are the observations of D from Table 12, while the open circles are ephemeris positions (0 TT) from the model.

ful solutions AE₁ and AE₂, displayed in Table 13. The residuals left by the latter solution are listed in Table 14. On account of the extremely small number of observations, either solution is deemed provisional, the second being slightly preferable.

The deletion of the (D–A) separation on April 9.8 from the set in Table 12 had a relatively minor effect on the fragmentation parameters, leading to Solution AD₃ also presented in Table 13; the revised list of residuals is in Table 15. It is noted that the removal of the data point from the 9th had, on the average, a beneficial effect on the residuals from other observations, the one on the 8th in particular. In the following I somewhat reluctantly adopt Fragment A as the most likely parent of D and Solution AD₃ as the latter’s best available fragmentation solution.

The reason for investigating only the scenario in which Fragment E derived from A was the availability of the (E–A) separations on three days. This data set, however humble, compares to a single occasion, on April 17, of the simultaneously observed Fragments B and E. The parent of Fragment E remains unclear and it is merely for the reasons already commented on in Section 3.3 that one can speculate that the most likely candidate for being its parent is Fragment A.

3.5. Relationship Among Fragments C, D, and E

The number of simultaneously observed (C, D) pairs is very limited. From the data in Tables 1 and 2, their total number is assessed at six. I have attempted a fragmentation solution to check whether Fragment D could have separated from Fragment C rather than from A (or B). The result, presented as Solution CD₁ in Table 16, is inconclusive. The acceleration in particular is determined with large uncertainty and no separation velocity could be detected. As shown in Table 17, two of the six observations could not be accommodated by the solution. There is no evidence that would point at a close relationship between Fragments C and D and at their separation from the parent as a single body.

Similar examinations of possible commonalities between Fragments C and E on the one hand and between Fragments D and E on the other hand cannot be undertaken because of the absence of reported simultaneous observations of either pair of these objects.

Table 13
Models for Motion of Fragment E and Revised Model for Motion of Fragment D
Relative to Fragment A of Comet C/2019 Y4

Parameter/Quantity	Solutions for Fragment E		Solution AD ₃ for Fragment D
	Solution AE ₁	Solution AE ₂	
Time of separation, $t_s - t_\pi$ (days)	-74.9 ± 2.5	-79.3 ± 3.2	-79.0 ± 5.2
Date of separation (UT)	2020 Mar 17.1	2020 Mar 12.7	2020 Mar 13.0
Heliocentric distance (AU)	1.74	1.81	1.81
Acceleration (10^{-5} solar gravity)	201 ± 25	173 ± 21	135 ± 32
Normal separation velocity (m s^{-1})	$+0.48 \pm 0.20$	-1.53 ± 0.45
Mean residual	$\pm 0''.56$	$\pm 0''.40$	$\pm 0''.76$
Number of observations	3	3	19

Note.

t_π is the perihelion time. Solutions for E are presented in the order of increasing number of parameters that were solved for. Normal separation velocity assumed to be zero is dotted. No solutions involving transverse and/or radial separation velocity components offered sets of meaningful parameters.

4. NUCLEAR FRAGMENTATION OF C/2019 Y4:
SUMMARY AND DISCUSSION

As pointed out in Section 1, the disintegration of comet C/2019 Y4 has not been entirely unexpected. Yet the process of its manifestation was rather unusual. I have remarked in Section 2 that the shape of the early portion of the nuclear-condensation's light curve looked very untypical. Until late January the *apparent* magnitude was constant, which, given that the comet was approaching both the Sun and Earth, meant that the *intrinsic* brightness was decreasing with time. The average rate of decline between late December and late January was actually rather steep, varying with heliocentric distance r approximately as $r^{4.5}$. Without the knowledge of the subsequent developments one could have guessed that the comet began to fade out already near 3 AU preperihelion. Since this clearly was not the case, the alternative and still potentially valid scenario could be that of the comet's light curve following a subsiding branch of an earlier outburst that took place prior to mid-December.

Under these circumstances, the comet's sudden and sustained brightening starting in late January looked as if the comet got a second wind. And since it is fairly common that an episode of nuclear splitting is accompanied by an outburst (e.g., Sekanina 2010), a prolonged brightening should, by extension, accompany a process of continual (recurring in rapid succession) or essentially continuous (uninterrupted) fragmentation over an extended period of time. If the particle velocity was rather low, new debris got into the inner coma before much of earlier one managed to leave it. Also, once the process started, the increasing energy input from the Sun, as the comet

kept approaching it, did facilitate debris release at ever higher rates.

This mode of fragmentation makes it difficult to model, because the resulting normalized nongravitational acceleration on the fragmenting object increases systematically with time at a high rate, as the object rapidly contracts. Application of a standard model that does not allow for this effect returns thus a value that represents a crude average over the relevant period of time.

4.1. Fragmentation Sequence

If the late January sudden change in the light curve of the nuclear condensation signaled a fragmentation event, it unquestionably was a breakup of the parent mass into Fragments A and B. Although the model failed to converge when the time of separation became one of the parameters to solve for, the distribution of residuals from the 33 used separations presented in Table 4 was de-

Table 15
Separations of Fragment D from Fragment A of C/2019 Y4 and
Revised Residuals from Solution AD₃ (Equinox J2000)

Time of observation 2020 (UT)	Separation D–A		Residual O–C		Obs. code
	in R.A.	in Decl.	in R.A.	in Decl.	
Apr 8.81700	+12''.3	–1''.2	+1''.5	+1''.8	K51
10.81943	+12.0	–4.1	–0.7	–1.5	A77
10.84504	+11.0	–2.9	–1.7	–0.3	204
11.87740	+14.1	–2.4	+0.4	0.0	C10
11.88527	+14.2	–2.4	+0.4	0.0	C10
11.89314	+15.3	–2.3	+1.5	+0.1	C10
11.90101	+14.1	–2.5	+0.3	–0.1	C10
11.90888	+13.9	–1.6	+0.1	+0.8	C10
13.18954	+14.2	–1.9	–1.1	+0.1	658
13.19262	+14.5	–2.8	–0.7	–0.8	658
13.19571	+14.5	–2.2	–0.7	–0.2	658
13.19880	+14.5	–2.6	–0.7	–0.6	658
13.20189	+15.3	–2.3	0.0	–0.3	658
13.86573	+15.9	–1.5	–0.2	+0.2	J95
13.86712	+15.5	–1.6	–0.6	+0.1	J77
13.88081	+16.9	–1.5	+0.8	+0.2	J95
14.86279	+17.9	–1.1	+0.6	+0.2	970
14.87810	+18.0	–1.0	+0.7	+0.3	970
14.90103	+17.5	–1.1	+0.2	+0.2	J95

Table 14

Separations of Fragment E from Fragment A of C/2019 Y4
and Residuals from Solution AE₂ (Equinox J2000)

Time of observation 2020 (UT)	Separation E–A		Residual O–C		Obs. code
	in R.A.	in Decl.	in R.A.	in Decl.	
Apr 9.80653	+10''.4	–0''.7	0''.0	–0''.2	K51
17.24276	+20.0	+2.6	–0.1	–0.4	F65
18.23496	+21.8	+4.3	+0.1	+0.5	F65

Table 16
Model for Motion of Fragment D Relative to Fragment C
of Comet C/2019 Y4

Parameter/Quantity	Solution CD ₁ for Fragment D
Time of separation, $t_s - t_\pi$ (days)	-60.1 ± 3.4
Date of separation (UT)	2020 Mar 31.9
Heliocentric distance (AU)	1.48
Acceleration (10^{-5} solar gravity)	214 ± 105
Mean residual	$\pm 0''.54$
Number of observations	4

Note.

t_π is the perihelion time. Solutions with more than two parameters were not attempted because it is unlikely that Fragment C is the parent to Fragment D. The very large uncertainty in the acceleration appears to support the absence of such a direct relationship between these fragments.

teriorating dramatically as the separation time was being moved forward. While the mean residual reached $\pm 0''.522$ for a separation time of 130 days before perihelion (from adopted Solution BA₁ in Table 3), it increased to $\pm 0''.528$ at 100 days before perihelion and to $\pm 0''.563$ at 70 days before perihelion. A formal minimum of $\pm 0''.518$ was reached 650 days before perihelion, an unrealistic solution.

Of the other fragments, the conclusion from the computations in the preceding sections is that separation from Fragment A was very probable for C, perhaps likely for D, and possible for E. Adopting for the three objects the fragmentation solutions of, respectively, AC₂ from Table 5, AD₃ from Table 13, and AE₂ from Table 13, one finds that D and E broke off essentially simultaneously, while C about a week later, but the C and D events were within 1σ of each other. These separation dates were centered on mid-March and approximately coincided with the sudden drop in the comet's *rate* of brightening, days before the light curves in Table 2 reached the peak.

Table 17
Separations of Fragment D from Fragment C of C/2019 Y4
and Residuals from Solution CD₁ (Equinox J2000)

Time of observation 2020 (UT)	Separation D–C		Residual ^a O–C		Obs. code
	in R.A.	in Decl.	in R.A.	in Decl.	
Apr 6.87924	+1''.1	–0''.5	+0''.4	–0''.4	970
11.83133	+2.2	–0.4	–0.8	–0.5	215 ^b
11.87207	+2.5	–1.9	(–0.4	–2.0)	B56 ^c
11.88748	+2.6	+3.6	(–0.3	+3.5)	585 ^d
13.86573	+4.2	+0.1	–0.2	–0.3	J95
13.88081	+5.1	+0.5	+0.7	+0.1	J95

Notes.

^a Entries whose residuals are parenthesized have been excluded from the solution.

^b Positions of fragments observed simultaneously at two codes: C at 215, D at G23.

^c Positions of fragments observed simultaneously at two codes: C at B56, D at Z30.

^d Positions of fragments observed simultaneously at two codes: C at 585, D at 938.

4.2. *Fragments' Detection, Activity, and Separation Trajectories*

Given that the duplicity of the comet's nucleus was not detected until early April, the breakup in late January meant that one component — the principal mass B, as it turned out — remained unobserved for at least 11 weeks. The disintegrating component A was the only part of the original nucleus — itself a companion — that was under observation continuously from the breakup until late April. In addition, the separation trajectory of Fragment A relative to B in Figure 3 suggests that in mid-March, when only A was seen, the two fragments were nearly 8'' apart, while by mid-April, when both A and B were observed, their separation diminished to less than 5''. The separation distance had obviously no effect on the detection of the duplicity. Instead, it was low activity of Fragment B prior to April that was keeping its brightness below the detection threshold of the telescopes used. It is likely that the HST would have been able to image the duplicity for most of the time it lasted, beginning not later than early February.

Interestingly, Fragments C, D, and E were all observed within four weeks or so of their presumed release from Fragment A, starting at separations of 10'' to 12''.

4.3. *Fragments' Nongravitational Accelerations, Lifetimes, and Relative Sizes*

The sublimation-driven nongravitational acceleration γ is an important fragmentation parameter, because it is determined by the physical properties of the fragment, just as in Whipple's (1950) model the nongravitational acceleration of a comet is determined by its physical properties. However, when the fragment's motion is measured relative to the parent nucleus, the derived value is a *differential* acceleration. The absolute acceleration of the fragment is the sum of its differential acceleration and the parent's acceleration.

The acceleration is statistically correlated with the fragment's lifespan, which is conveniently measured by the endurance, \mathcal{E} , defined as the difference between the separation time and the time of last observation, reduced to a normalized heliocentric distance of 1 AU, and expressed in equivalent days (or e-days). For comets in nearly-parabolic orbits (Sekana 1982)

$$\mathcal{E} = 40.5 q^{-\frac{1}{2}} (u_{\text{fin}} - u_{\text{frg}}), \quad (9)$$

where q is the perihelion distance (in AU) and u_{frg} and u_{fin} are the true anomalies (in radians) at the times of separation and final observation, respectively. Because of effects due to observing conditions, the measured lifespan is in general a lower limit to the true lifespan.

The limited statistics of two dozen data points suggest the existence of three basic categories of cometary fragments: *persistent*, *short-lived*, and *minor* (Sekana 1982). As already noted in Section 1, the endurance was found to vary with the acceleration as

$$\mathcal{E} = C \gamma^{-0.4}, \quad (10)$$

where $C = 800$ e-days for the most massive, persistent fragments, 200 e-days for the short-lived fragments, and 87 e-days for the minor fragments.

From Solutions BA₁, AC₂, AD₃, and AE₂ one finds, in units of 10^{-5} the solar gravitational acceleration, the

nongravitational accelerations of 21.7 ± 2.8 for Fragment A relative to B and 161 ± 30 , 135 ± 32 , and 173 ± 21 , respectively, for Fragments C, D, and E relative to A. Fragment A is positively a short-lived fragment, whose acceleration implies an endurance of 58 ± 3 e-days. The other fragments are apparently short lived as well, in which case the endurances equal 26.2 ± 2.0 e-days for Fragment C, 28.1 ± 2.7 e-days for D, and 25.5 ± 1.2 e-days for E. Should they be minor fragments, their endurances would be too short: 10.8 ± 0.8 e-days, 11.5 ± 1.1 e-days, and 10.6 ± 0.5 e-days, respectively.

These numbers apply on the assumption that the principal mass B was affected by no nongravitational acceleration. As the comet was itself a companion fragment of a larger comet, this is unlikely to be the case. Indeed, the orbit computed by the MPC Staff (2020) indicates that between 20 December 2019 and 3 April 2020 the comet's motion was affected by a strong nongravitational acceleration. Of course, if the nucleus split into Fragments A and B around 22 January, the MPC elements timewise cover only 31 percent of the motion of the pre-split nucleus and 69 percent of the motion of Fragment A, as Fragment B was not seen until after 3 April. As the MPC Staff determined the orbit using Marsden et al.'s (1973) model with the standard $g(r)$ nongravitational law, it is necessary to convert the integrated effect of the radial sublimation-driven force from the Marsden et al. nomenclature to the style used in this paper.

The fundamental condition to be satisfied is that the dominant nongravitational effect in the radial direction, whose magnitude in the period from 20 December to 3 April was measured in the MPC Staff's (2020) orbital solution by a parameter $A_1 = +16.16 \times 10^{-8}$ AU day $^{-2}$, be equated with the sum of the radial nongravitational effects, expressed in the style used in this paper, (i) on the pre-split nucleus between 20 December and 22 January, defined by a parameter γ_{par} ; *plus* (ii) on Fragment A between 22 January and 3 April. The latter part consists of the total radial nongravitational effect on Fragment B, defined by a parameter γ_{b} ; *plus* the radial nongravitational effect on Fragment A relative to B, defined by the tabulated parameter $\gamma_{\text{ba}} = 21.7$ units of 10^{-5} the solar gravitational acceleration. The condition thus reads

$$\int_{t_{\text{beg}}}^{t_{\text{end}}} A_1 g(r) dt = \int_{t_{\text{beg}}}^{t_{\text{frg}}} \gamma_{\text{par}} \Gamma_{\odot} \left(\frac{r_{\oplus}}{r} \right)^2 dt + \int_{t_{\text{frg}}}^{t_{\text{end}}} (\gamma_{\text{b}} + \gamma_{\text{ba}}) \Gamma_{\odot} \left(\frac{r_{\oplus}}{r} \right)^2 dt, \quad (11)$$

where t_{beg} , t_{end} , and t_{frg} are, respectively, the times of the beginning and the end of the orbital arc, integrated by the MPC Staff (2020), and the time of fragmentation. Expressed in days from perihelion, they are equal to $t_{\text{beg}} = -163$ days, $t_{\text{end}} = -58$ days, and, as adopted, $t_{\text{frg}} = -130$ days; $r_{\oplus} = 1$ AU, so that γ_{par} and γ_{b} refer to 1 AU and, like γ_{ba} , are in units of 10^{-5} the solar gravitational acceleration; at 1 AU from the Sun this unit equals $\Gamma_{\odot} = 0.593 \times 10^{-5}$ cm s $^{-2} = 0.296 \times 10^{-8}$ AU day $^{-2}$. Employing Kepler's Second Law and elementary operations, and leaving r_{\oplus} out, Equation (11) can be rewritten thus:

$$A_1 \mathfrak{S}_{\text{beg, end}} = \Gamma_{\odot} [\gamma_{\text{par}} (u_{\text{frg}} - u_{\text{beg}}) + (\gamma_{\text{b}} + \gamma_{\text{ba}}) (u_{\text{end}} - u_{\text{frg}})], \quad (12)$$

where u_{beg} , u_{end} , and u_{frg} are the true anomalies (in radians) at, respectively, t_{beg} , t_{end} , and t_{frg} ; and

$$\mathfrak{S}_{\text{beg, end}} = \int_{u_{\text{beg}}}^{u_{\text{end}}} r^2 g(r) du = \int_{r_{\text{end}}}^{r_{\text{beg}}} r \left(\frac{r}{q} - 1 \right)^{-\frac{1}{2}} g(r) dr. \quad (13)$$

The integration over r , with $r_x = r(t_x)$, is a parabolic approximation valid on the assumption that $u_{\text{beg}} < 0$ and $u_{\text{end}} < 0$.

The condition (12) includes two unknowns: γ_{par} and γ_{b} . Its solution requires an additional condition on the two accelerations. If the parent and Fragment B were about equally active, one would expect that $\gamma_{\text{par}} < \gamma_{\text{b}}$, the two values the closer to each other the smaller Fragment A relative to B. Because Fragment A was much more active than B, it is likely that in relative terms the parent was more active than Fragment B, in which case γ_{par} could equal γ_{b} or even exceed it. As a first-guess estimate I assume equality, in which case condition (12) becomes

$$\gamma_{\text{par}} = \gamma_{\text{b}} = \frac{3.38 \times 10^8 A_1 \mathfrak{S}_{\text{beg, end}} - \gamma_{\text{ba}} (u_{\text{end}} - u_{\text{frg}})}{u_{\text{end}} - u_{\text{beg}}}. \quad (14)$$

For the considered MPC orbit, $u_{\text{end}} - u_{\text{beg}} = 0.2813$ radian, $u_{\text{end}} - u_{\text{frg}} = 0.2304$ radian, and from Equation (13) $\mathfrak{S}_{\text{beg, end}} = 0.1167$ AU 2 , so that

$$\gamma_{\text{par}} = \gamma_{\text{b}} = 4.9 \text{ units of } 10^{-5} \text{ solar grav. accel.} \quad (15)$$

More generally, one could assume

$$\gamma_{\text{b}} = g \gamma_{\text{par}}, \quad (16)$$

where $g > 0$ and $g \neq 1$. The solution (14) is now slightly modified,

$$\gamma_{\text{par}} = \frac{3.38 \times 10^8 A_1 \mathfrak{S}_{\text{beg, end}} - \gamma_{\text{ba}} (u_{\text{end}} - u_{\text{frg}})}{(u_{\text{end}} - u_{\text{beg}}) + (g - 1)(u_{\text{end}} - u_{\text{frg}})}. \quad (17)$$

One can show that if $\gamma_{\text{par}} = \gamma_{\text{b}} > 0$, then $\gamma_{\text{par}} > 0$ and $\gamma_{\text{b}} > 0$ for any $g > 0$. The only condition for $\gamma_{\text{par}} > 0$ is a constraint on the ratio of γ_{ba} to A_1 ,

$$\frac{\gamma_{\text{ba}}}{A_1} < \frac{3.38 \times 10^8 \mathfrak{S}_{\text{beg, end}}}{u_{\text{end}} - u_{\text{frg}}}, \quad (18)$$

where the units are, as above, 10^{-5} the solar gravitational acceleration for γ_{ba} and AU day $^{-2}$ for A_1 .

Limited experimentation with the factor g suggests that for values moderately exceeding, or slightly lower than, unity, the accelerations γ_{par} and γ_{b} do not differ from (15) by more than a few units of 10^{-5} the solar gravitational acceleration. As seen, γ_{b} is about a factor of 4 to 5 smaller than γ_{ba} and does not amount to more than a few percent (well within the uncertainty) of the high nongravitational accelerations that Fragments C, D, and E are subjected to.

Turning back to the lifespan of the fragments, I note that by eliminating the endurance from Equations (9) and (10) it is possible to approximately predict the time of final observation of a fragment, t_{fin} , from the model parameters — the time of separation, t_{frg} , and the nongravitational acceleration, γ — when the fragment's category (persistent, short-lived, or minor), determining the parameter C , is known. The prediction can be tested on

Table 18
Lifespans of C/2019 Y4 and Its Fragments

Object/ fragment	Time of separation (2020 UT)	Nongravitational acceleration γ (units ^a)	Endurance \mathcal{E} (e-days)	Fragment category	Last sighting (2020 UT)		
					predicted	reported	source ^b
Parent/B	previous perihelion ^c	5	420 105	persistent short-lived	May 24	May 21	COBS
A	Jan 22	21.7 28 ^d	58 53	short-lived short-lived	May 11 May 8	Apr 23	HST
C	Mar 20	161	26.2 10.2	short-lived minor	Apr 30 Apr 13	May 2	MPC
D	Mar 13	135	28.1 11.5	short-lived minor	Apr 29 Apr 9	Apr 23	HST
E	Mar 12	173	25.5 10.6	short-lived minor	Apr 27 Apr 8	(Apr 18)	MPC

Notes.

^a Units of 10^{-5} the solar gravitational acceleration; at 1 AU from the Sun 1 unit is equivalent to 0.296×10^{-8} AU day⁻².

^b Abbreviations: COBS = Comet Observation Database, Črni Vrh Observatory, near Idrija, Slovenia (<https://www.cobs.si/analysis>); HST = Hubble Space Telescope (Ye et al. 2021); MPC = IAU Minor Planet Center, Cambridge, Massachusetts (MPC Staff 2020).

^c Previous perihelion of the parent comet of C/1844 Y1 and C/2019 Y4 is believed to have taken place several thousand years ago.

^d The value includes an estimated contribution from the acceleration that the parent/Fragment B was subjected to.

the data available from observations. In a parabolic approximation, adequate for this purpose, the procedure includes three steps as follows:

$$\begin{aligned}
 u_{\text{fin}} &= u_{\text{frg}} + 0.0247 C q^{\frac{1}{2}} \gamma^{-\frac{2}{5}}, \\
 r_{\text{fin}} &= \frac{q}{\cos^2 \frac{1}{2} u_{\text{fin}}}, \\
 t_{\text{fin}} - t_{\pi} &= \mp 27.404 (r_{\text{fin}} + 2q)(r_{\text{fin}} - q)^{\frac{1}{2}}, \quad (19)
 \end{aligned}$$

where t_{π} is the time of perihelion. As before, the true anomalies are in radians, the distances in AU, and the times in days, the signs giving t_{fin} before/after perihelion.

The predicted dates of last sighting are compared in Table 18 with the reported times. The agreement is fairly good, when appropriate fragment categories are assigned. This is dramatically seen in the case of the principal fragment B, the most massive part of the pre-split comet, a companion to the Great Comet of 1844, as already noted. Let us assume that the two comets separated from their parent at the time of previous perihelion, several thousand years ago. If C/2019 Y4 should have survived as a persistent fragment until the 2020 perihelion, its endurance would have been 506 e-days. From γ_{par} in Equation (15) its endurance is expected to equal 420 e-days, last observed just 86 e-days short of the full revolution, a period of time equivalent to ~ 7 days. Since the endurance varies as time weighted by r^{-2} , the ratio $86/7 \simeq 12.3$ is, as it should be, about halfway between $(1/0.34)^2 \simeq 8.7$, where 0.34 AU was the heliocentric distance on May 24, and $(1/0.25)^2 = 16$, where 0.25 AU was the perihelion distance on May 31. If the comet were instead a short-lived fragment, its endurance would have been only a little more than 100 e-days and it would have fragmented and disintegrated at some point after the previous perihelion, on its way to, and long before reaching, aphelion. C/2019 Y4 would never have been discovered.

By contrast, Fragment A was a short-lived fragment, which should have lasted until early to nearly mid-May. Of the few data sources that I inspected, it was the last time seen in the images taken with the HST on 23 April and its lifespan must have been longer than that. The three fragments that separated, presumably from A, around mid-March, were obviously also short lived. They could not have been minor fragments, given that they were observed after 8–13 April.

Even though the definition of the *last sighting* is not straightforward, the introduction of the endurance is very beneficial in that it offers some insight into the morphology of comet fragmentation products and demonstrates that the sublimation-driven nongravitational acceleration has important physical implications in more than one respect.

The disintegration time of a sizable fragment differs from the disintegration time of a comet as such. The laws of cascading fragmentation imply that a comet's particulate debris survives and is detectable as a fairly condensed cloud over a period distinctly longer than the individual massive fragments because the debris has a much higher ratio of cross-sectional area to mass. There is nothing controversial, especially among comets of small perihelion distance, about large fragments dissolving before, while the comet's remains after, perihelion. Indeed, C/2019 Y4 was reported to have been detected by the HI-1 imager of STEREO A as late as 6 June (Knight & Battams 2020), about a week following perihelion.

An important property of the nongravitational acceleration of a fragment is that it serves as a crude size estimate of the object. The acceleration varies as the mass-loss rate of sublimated gas from its surface and inversely as the object's mass. The mass-loss rate varies as the square of the size, while the mass as the cube of the size. Accordingly, the nongravitational acceleration varies inversely as the size.

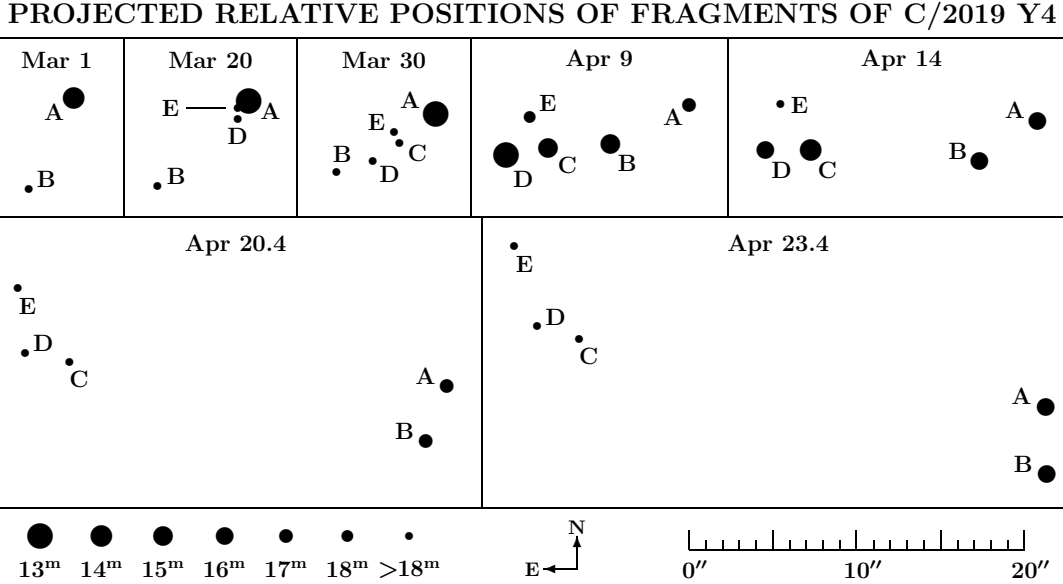


Figure 8. Relative positions of the fragments of comet C/2019 Y4 on seven dates between 1 March and 23 April 2020. The times for the first five dates are 0 UT, for the last two dates they approximately coincide with the times of the HST imaging. The positions have been derived from Solutions BA₁, AC₂, AD₃, and AE₂. The size of each magnitude symbol, assigned for orientation purposes only, is an approximate match to an average daily nuclear brightness reported to the MPC; a fragment that was not reported is usually assumed to have been too faint to detect (of magnitude >18). The scale and orientation (the north up, east to the left) are also shown.

One can of course think of variations on the basic sublimation model, including the nuclear shape, rotation, etc. For example, the following empirical relation approximates a link between the acceleration γ (again in units of 10^{-5} the solar gravitational acceleration) and the fragment’s initial diameter D (in km) implied by a slightly more complex model (Sekanina 1982):

$$D = 2.16 \gamma^{-0.92}. \quad (20)$$

For the pre-split nucleus of C/2019 Y4 this law gives an effective initial diameter of 500 meters, for Fragment A about 100 meters, and for Fragments C, D, and E between 16–20 meters.

4.4. Projected Relative Positions of Fragments As Function of Time

The fragmentation sequence of C/2019 Y4, jointly with the peculiar separation trajectory of Fragment A relative to B (Figure 3), are behind the rather intricate motions of the individual fragments relative to one another in projection onto the plane of the sky. The picture is further complicated by their rapid and irregular brightness variations.

The projected relative positions of the five fragments as a function of time are illustrated in Figure 8 by their status on seven selected dates, including the two on which the disintegrating comet was imaged by the HST. A particularly confusing situation is seen to have developed in early April, when the multiplicity was first detected. The three more recently born fragments were moving in a general direction of the line connecting the formerly existing Fragments A and B, not to mention that it was at this very time that B suddenly became bright enough to detect. Subsequently, the high nongravitational accelerations of C, D, and E caused the rapid eastward motions of these fragments away from A and B.

5. ORBIT OF THE GREAT COMET OF 1844

The early history of major effort to determine the orbit of comet C/1844 Y1 was a little wobbly. The first to get involved was Bond (1850), in part because he wanted to examine the possible identity of this object with the comet of 1556. Bond collected 138 astrometric observations of the comet made between 24 December 1844 and 12 March 1845, organizing them into seven normal places. He then selected 1 January 1845 as an osculation epoch and accounted for the perturbations by the “principal” planets. The result was a set of hyperbolic elements with a perihelion distance of 0.2517170 AU and an eccentricity of 1.00035303. Bond did not compute the standard errors of the orbital elements, but his table of residuals for the normal places implies a mean residual of $\pm 4''.4$.

Sixty years later, Fayet (1910) reviewed Bond’s orbital work on this comet and discovered a serious mistake in the equations of condition in declination (or, rather, in the polar distance that Bond actually worked with). The net result of Fayet’s reexamination was an elliptic orbit, with a perihelion distance of 0.2508701 AU and an eccentricity of 0.9997302; again, no errors of the elements were provided. The corresponding osculating orbital period was about 28,000 yr. Fayet did not compute the original period, but it is highly unlikely that it would have come out much shorter than the osculating value. In addition, Fayet also derived a parabolic solution, whose fit to the observations was only marginally worse, so slightly in fact that Marsden (1972) incorporated the parabola into the first edition of his *Catalogue of Cometary Orbits*, mentioning the ellipse only in the notes.

I got interested in the physical behavior of C/1844 Y1 as part of my extensive investigation of anomalous tails (or antitails) of comets in 1974 (Section 6). At the time I wanted to learn whether the astrometric observations

were adequate for determining whether the comet could be a member of the Oort Cloud and decided to calculate its orbit from scratch. Unlike Bond and Fayet, I employed only the most consistent positional data that left residuals not exceeding $\pm 3''$, which restricted their total number to merely 41, or 30 percent of the number collected by Bond. The outcome of my effort was first listed (as unpublished) in the second edition of Marsden’s (1975) *Catalogue* and eventually incorporated into the summary paper by Marsden et al. (1978). The solution left a mean residual of $\pm 1''.81$, suggesting the comet’s original orbital period of 7600 ± 1100 yr. While there is no doubt that C/1844 Y1 was not an Oort Cloud comet, the mean error of about 15 percent of the orbital period is uncomfortably high for the present study.

More recently, S. Nakano (Green 2020a) reported a new orbital determination of the comet by T. Kobayashi, who used another set of 41 observations that left a mean residual as high as $\pm 5''.2$. The osculating orbital period came out to equal 3720 yr, corresponding to an original orbital period of 4000 yr, more than 3σ shorter than the orbit I had derived in 1974. The high mean residual makes the new orbit suspect and, in any case, the discrepancy between the two results allows one only to conclude that the comet returned to perihelion after several thousand years. The orbital periods derived for C/2019 Y4 are of little value because of the complications caused by the major nongravitational effects (Marsden et al. 1973).

6. GREAT COMET OF 1844 AND ITS ANTITAIL

The comet, which suddenly burst into sight as a naked-eye object about 4 days after perihelion, was referred to either as the Great Comet of 1844 (or 1844/1845) or as comet Wilmot. The last name was based on the strength of Maclear’s (1845a) dubious claim that the comet was “first seen by Captain Wilmot,” subsequently corrected by Maclear (1845b) himself.

In connection with my research on comet Kohoutek, C/1973 E1 (Sekanina 1973, 1974a; Sekanina & Miller 1976), I realized that the conditions for displaying a tail projecting *sunward* and consisting exclusively of large particulates (typically >100 microns across), could be *predicted* for any comet sufficiently rich in dust. A feature of this kind is referred to as an *anomalous tail* or, shortly, an *antitail*. In the subsequent investigations of antitails (e.g., Sekanina 1974b, 1976), I determined that C/1844 Y1 was one of the objects for which favorable conditions to display an antitail extended over a number of days centered on the time of the Earth’s transit across the comet’s orbital plane. The longitudes of the Earth and the comet’s ascending node coincided on 1845 January 18.6 UT, 5 days before the full Moon.

I was able to locate two independent references to the antitail’s detection in the relevant period of time. One was a report by Maclear (1845b), Cape Observatory, who described the appearance of the comet on January 11: “[A] faint ray of luminous matter, about $1\frac{1}{4}$ degree in length, was seen to extend from the anterior portion of the comet’s head in a direction opposite to that of the tail. The breadth of this ray near the head was about $2'$, increasing slightly towards the extremity. Its borders were comparatively well defined, and the light gradually diminished in intensity from that portion nearest the comet’s head, until it became insensible.”

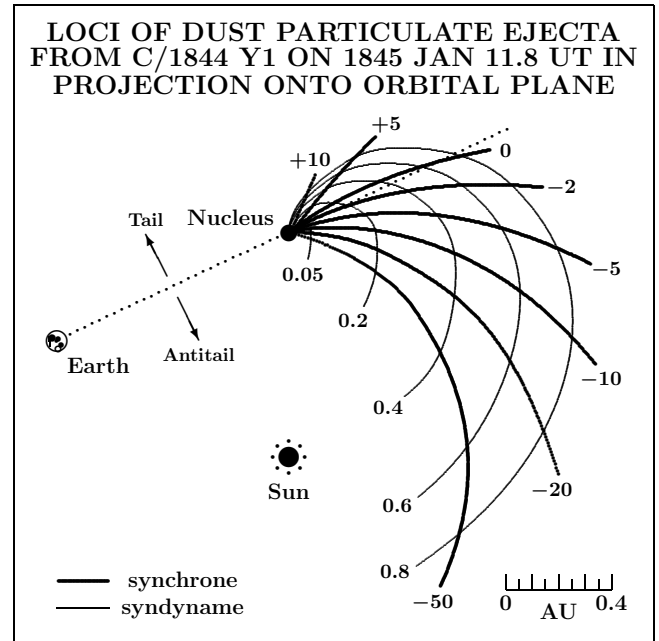


Figure 9. Synchrones and syndynames of dust ejected from the nucleus of comet C/1844 Y1 for the time of observation by T. Maclear on 1845 Jan 11.8 UT in projection onto the orbital plane of the comet. The synchrones are the thick curves, each marked by the time of ejection from the nucleus measured in days from perihelion (1844 Dec 14.2 UT). They cover a period of time from 50 days before perihelion (1844 Oct 25; -50) to 10 days after perihelion (1844 Dec 24; $+10$). The age of a synchrone at the time of observation is derived by subtracting the marked ejection time from 28.6 days. The syndynames are the thin curves, each providing the magnitude of the solar radiation pressure acceleration β affecting the particles and confined in the plot to a range from 0.05 to 0.8 the solar gravitational acceleration. Particle size varies inversely as the magnitude of the radiation pressure effect. Note that, as seen from the Earth, larger particles ($\beta < 0.2$) ejected earlier than about 2 days before perihelion project at the time of observation on the sunward side of the comet’s head as an antitail. In practice, the visible antitail consists only of large particles whose $\beta < 0.05$ (Table 19 and the text). Also note that microscopic grains ($\beta > 0.6$) released from the comet before late October 1844 were at the time of observation located on the other side of the Sun from the comet. These grains were scattered too widely in space to be detected. The Earth was at the time 0.085 AU above, and moving towards, the comet’s orbital plane, transiting it 7 days later.

Maclear then continued: “From the 18th to the 27th, the tail and the anterior ray were both rendered invisible by the moonlight. Viewed with the comet-sweeper on the latter evening, the northern border of the . . . anterior ray appeared distinct and sharply defined, but [its] southern border could no longer be traced. . . Viewed with the 46-inch achromatic, . . . the anterior extension of the light could be traced as a distinct ray for about $5'$ from the comet’s head, the luminous matter on the southern border becoming then diffused and scattered, while the northern border continued well defined.”

The meaning of Maclear’s statements is clarified below with help of (i) a plot of the dust ejecta’s modeled distribution in the comet’s orbital plane, presented in Figure 9; and (ii) the antitail’s predicted length and orientation as a function of the ejection time, shown in Table 19. But first I offer the details of the other published account, by Waterston (1845), who reported from Bombay, India, that the comet displayed “a singular luminous

Table 19
 Predicted Lengths and Position Angles of Antitail of C/1844 Y1 As Function of Ejection Time For Several Times of Observation

Time of observation 1845 (UT)	Distance of Earth from orbit plane of comet ^a (AU)	Position angle of Sun	Dust particles subjected to $0 < \beta \leq 0.02$ and ejected at time t_{ejec} before perihelion ^b									
			$t_{\text{ejec}} = 50$ days		$t_{\text{ejec}} = 20$ days		$t_{\text{ejec}} = 10$ days		$t_{\text{ejec}} = 5$ days		$t_{\text{ejec}} = 0$ days	
			Length	P.A.	Length	P.A.	Length	P.A.	Length	P.A.	Length	P.A.
Jan 11.8	+0.085	275°6	1°35	283°5	0°90	287°6	0°54	295°1	0°23	320°5	0°27	74°0
16.5	+0.026	269.8	1.49	272.1	1.07	273.1	0.72	274.8	0.34	279.3	0.17	77.2
18.6	0.000	267.7	1.54	267.7	1.15	267.7	0.80	267.7	0.42	267.7	0.12	87.7
25.5	-0.086	263.5	1.68	256.6	1.39	254.4	1.09	251.4	0.72	246.1	0.16	198.3
29.8	-0.139	262.3	1.73	251.6	1.50	248.6	1.25	244.9	0.91	239.0	0.31	208.2
Feb 1.8	-0.175	261.9	1.75	248.8	1.57	245.4	1.35	241.3	1.03	235.4	0.42	210.2

Notes.

^a Plus sign means Earth was above the comet’s orbit plane (in the comet’s coordinate system) and vice versa.

^b At low radiation pressure accelerations, length varies essentially as the upper limit of β .

appendage, which, on the evening of [January] 16th (on about 16.55 UT) I observed for the first time to proceed from the head of the comet towards the Sun almost diametrically opposite to the proper tail. It consisted of a narrow band of faint light of about the same breadth as the head. The edges were well defined and parallel. It could be traced for 3° , and probably extended much farther, as the increasing moonlight was very unfavorable to so faint an object. ... [O]n the evening of [January] 25th [t]he two tails ... made an evident angle, and the space was filled with a diffused, irregular light, giving a triangular shape to the comet when seen by the naked eye ... This evening (the day not given, but before January 31), the same appearance continues, but very faint, the angle at the head of the comet being about 140° .”

Waterston also wrote a popular article about comet C/1844 Y1 and its antitail in the *Bombay Courier*. It was published on 1845 January 21 and copied by Pole (1845) in his paper on the comet. While it does repeat some of the above lines, it is informative enough to warrant a brief extract. Waterston wrote: “There is a very remarkable appearance attending upon this Comet ... It has got two tails!! The second tail, which is nearly in an opposite direction to the principal one, was first seen on ... 16 January and has continued visible ever since, although the increasing moonlight is very unfavorable. It is extremely faint, but has been recognized by several persons, and I have traced it distinctly for about 3° towards the sun ...”

The attentive reader will note a major weakness of the narratives by Maclear and Waterston in that they include no accurate data on the orientation of the antitail and little information on its length. Such data should narrow down the wide ranges of parametric values of the model. In fact, a few data of this kind — specifically, the position angles of the northern border of the antitail, which Maclear referred to as the anterior luminous matter — were published in another paper by Maclear (1845c); the measurements were actually made by his assistant at the Cape Observatory, W. Mann. The issue with these measurements is that they make no sense, a problem whose ultimate solution brings me first to explaining the meaning of Maclear’s and Waterston’s descriptions of the feature’s observed properties.

The systems of synchrones and syndynames in Figure 9 indicate that, on the condition of a zero ejection velocity, the position of a released dust particle at a given time depends on the time of ejection, t_{ejec} , and the magnitude of the solar radiation pressure, β , it is subjected to. The value of β is a function of the particle’s physical and optical properties. For large particles (tens of microns and larger), β varies inversely as the product of their size and bulk density. For an assumed bulk density of 0.5 g cm^{-3} , the particle’s effective diameter \mathcal{D}_p (in microns) equals

$$\mathcal{D}_p = \frac{2.3}{\beta}, \quad (21)$$

where β is in units of the solar gravitational acceleration. The numbers in Table 19 apply to dust particles larger than 115 microns across.

The plot in Figure 9, depicting the field of dust ejecta in the comet’s orbital plane as it appeared at the time of Maclear’s first detection of the antitail, is remarkable in a number of ways. It often is stated that an antitail’s sunward direction is in its entirety an effect of projection and that in space the antitail actually points away from the Sun. Figure 9 shows that this clearly is not the case here. Particles ejected 50 days before perihelion are at the time of observation obviously closer to the Sun than the comet and the ones smaller than about 4 microns across are actually located on the other side from the Sun. Of course these particles are too scattered in space to be seen. It is only the large particles, having very low values of β and coming mostly from near-perihelion ejections that Maclear reported. These in Figure 9 populate an area that is a little farther from the Sun than the comet. The dotted line connecting the Earth with the comet’s nucleus shows that, as seen on 11 January, all large particles ejected earlier than about 2 days before perihelion ended up in the antitail.

Since Maclear provided information on both the length and width of the antitail on 11 January, one can learn additional information on the ejecta from Table 19. For example, if the dominant contribution came from the dust ejected approximately 5 days before perihelion, particles as small as about 20 microns in diameter could have been located at the terminal point of the feature. If the pre-

Table 20
Orientations of the Principal Tail and Antitail and Contributing Dust Ejecta
of C/1844 Y1 from Corrected Measurements by W. Mann

Time of observation 1845 (UT)	Principal tail		Antitail		Angle subtended by tails
	Measured P.A. of axis	Effective ejection time (days ^a)	Measured P.A. of N border	Effective ejection time (days ^a)	
Jan 29.8	94°4	+8.9	238°9	−5.4	144°5
30.8	92.8	+13.9	241.5	−8.2	148.7
31.8	90.9	+13.9	238.2	−6.5	147.3
Feb 1.8	94.8	+11.7	235	−5.3	140

Note.

^a Ejection time measured from perihelion, 1844 Dec 14.2 UT; negative sign means before perihelion, positive sign after perihelion.

vailing ejecta were of much older age, close to 80 days, the antitail should have contained only dust grains whose diameter exceeded 120 microns.

No less interesting conclusion follows from Maclear’s estimate of the antitail’s width, which can be interpreted in one of two ways. Since 2′ is equivalent to an arc of 1°.5 at a distance of 75′, the estimated width could be generated by the ejections continuing over a period of merely 0.3 day if the dust was ejected 5 to 10 days before perihelion, but over some 11 days if between 20 and 50 days before perihelion. Assuming an exceptionally brief outburst, the same width should be due to an ejection velocity normal to the orbit plane. One then obtains for the upper limit of this velocity a value between 6 and 16 m s^{−1}, depending on the time of ejection. In reality, the outburst scenario is extremely unlikely and the interpretation in terms of extended activity must be the correct one, implying a very low ejection velocity, perhaps of about 1 m s^{−1} or so. Its true magnitude should more accurately be determined from the antitail’s width at the time of the Earth’s transit across the comet’s orbital plane. Unfortunately, the feature was then invisible on account of the strong moonlight.

The adopted explanation of the antitail’s width as an effect of continuous production of dust is also consistent with Waterston’s account of the comet’s appearance on 25 January, when he noted the diffuse light filling the space between the antitail and the principal tail. This feature confirms that the emission of dust was continuous and that it was missed by Maclear only because of the ejecta’s extremely low surface brightness.

Related to this issue is the comment that Maclear made with respect to his observation of the antitail’s borders on 27 January in the comet sweeper and the large telescope. He noted that the northern border was sharply defined, whereas the southern border was diffused. From Table 19 it is obvious that the northern border was made up of the earliest ejecta that the observer was able to detect, whereas the southern border consisted of the most recent ejecta that he could recognize, given the surface-brightness thresholds of his instruments. It should be emphasized that before the Earth crossed the comet’s orbital plane, the roles of the two borders had been interchanged: the southern border had been then the one populated by the earliest ejecta.

I now come back to the controversial position angle observations by Mann (Maclear 1845c), the only ones of the kind that I was able to find. The published data refer to the axis of the principal tail and to the northern (sharper) border of the antitail on each of the four nights between 29 January and 1 February. While it is remarkable that the feature could still be measured at all two weeks after the orbital plane’s transit, Mann’s nominal position angles of the antitail’s border on the four nights, equaling 301°.1, 298°.5, 301°.8, and 305°, respectively, cannot be correct, because the northern border was in the third, not fourth, quarter. If Mann measured the position angle from the parallel, it could be that the term “northern” misled him to erroneously add — rather than subtract — the angle that the border subtended with the direction to the west. If so, the correct position angles of the antitail’s northern border, PA_{corr}, are related to its published values, PA_{publ}, by PA_{corr} = 540° − PA_{publ}. That this explanation of the meaningless numbers is plausible appears to be documented by comparing the angle of 140° between the two tails, reported at approximately the same time by Waterston, with the same angle, computed from Mann’s measurements to equal 144°.5 after correction but 153°.3 before it.

Table 20 lists Mann’s measured position angle of the principal tail’s axis, the corrected position angle of the antitail’s northern border, the angle they subtend, and the effective times of ejection corresponding to the respective position angles. These times were derived from the computed position angles of a system of synchrones. The telescopic measurements, which obviously referred to the orientations of the axis and border near the comet’s nucleus, were compared to the model values at very low accelerations β . The results, based on the observations made between 29 January and 1 February, suggest that the earliest ejecta in the *observed* antitail were large grains (mostly exceeding 100 microns in diameter), released, on the average, about 5 days before perihelion, whereas the major contribution to the principal tail was the microscopic (micron-sized) dust ejected at times centered approximately on 12 days after perihelion. Accordingly, much of the material in the two tails and in space between them derived from dust ejections that extended over a little longer than two weeks asymmetrically centered on perihelion.

Finally, the antitail observations provide evidence of the comet's fairly high rate of dust production before perihelion. One may have questioned the level of this activity, given that the comet was not discovered until after perihelion. However, the reason for the failure was the extremely unfavorable preperihelion observing conditions, with the comet staying at solar elongations not exceeding 35° between 3 AU from the Sun in early July 1844 and perihelion.

7. PAIR OF C/1844 Y1 AND C/2019 Y4 AS EXTREME CASE AMONG KNOWN LONG-PERIOD COMET GROUPS

The pair of C/1844 Y1 and C/2019 Y4 extends the very limited number of groups of long-period comets in nearly identical orbits, undoubtedly products of relatively recent nucleus fragmentation. The largest and best known among these groups is a foursome headed by the principal fragment C/1988 A1 (Liller) and comprising the companion fragments C/1996 Q1 (Tabur), C/2015 F3 (SWAN), and C/2019 Y1 (ATLAS). It was sheer coincidence that the group's most recent member happened to be discovered by the ATLAS project less than two weeks prior to C/2019 Y4.

The Liller group is the only one known to have more than two members. Before the discovery of C/2019 Y4, the best defined pair consisted of C/1988 F1 (Levy), the principal fragment, and C/1988 J1 (Shoemaker-Holt), the companion fragment. Of the two additional, probable pairs that should be mentioned, one includes C/1915 R1 (Mellish) and C/2016 R3 (Borisov) and is unusual in more than one respect. The orbits differ from each other a little more than in the other instances, but this could be because of a poorly determined orbit of comet Mellish (Williams 2016). Rather peculiar, but entirely coincidental is that the two objects arrived at the same time of the year to within three days under equally unfavorable conditions. Both were astrometrically observed over very limited periods of time before perihelion, Mellish over just 4 days, Borisov some two weeks. Neither was picked up after perihelion, although under ordinary circumstances they should have been, in the southern hemisphere (Einersson 1915, Aitken 1915, Green 2016). It is significant that attempts to link the motions of the two comets failed (Williams 2016), so these were not returns of the same object. It is possible that neither Mellish nor Borisov survived perihelion and that — unlike in the above three examples — *both comets were companion fragments to an unknown principal fragment* that had passed perihelion unobserved many decades before 1915. An approximate original orbital period for comet Borisov equals 2330 ± 880 yr.¹

The other probable pair is linked to the story of the so-called Lick Object, a very unusual phenomenon observed near the setting Sun by a party at the residence of the Lick Observatory Director W. W. Campbell on 7 August 1921. The event, described in the literature (Campbell 1921a, 1921b) and corroborated by a few independent reports, was believed to be most probably an unknown comet. A recent detailed investigation by Sekanina & Kracht (2016) led to a conclusion that the Lick Object apparently was a fragment of a comet that it had shared with the sunskirter C/1847 C1 (Hind).

7.1. Fragments' Returns to Perihelion and Orbital Periods

The data on the groups of long-period comets, presented in Table 21 to be discussed in Section 7.2, display some interesting features. The term *long period* is defined by the range of original orbital periods of the four groups, whose principal fragments are known. According to the catalogue by Marsden & Williams (2008), the periods varied from ~ 2900 yr for comet Liller to $\sim 14,000$ yr for comet Levy. The Great Comet of 1844 and comet Hind had intermediate periods of 7600 yr and 8300 yr, respectively. The typical original orbital period is thus on the order of several thousand years, with a maximum-to-minimum ratio of approximately 5:1.

The appearance of the principal and companion fragments, the order of return to perihelion, and the range of time lags between the principal and companion fragments among these long-period comets vary so strikingly that there must be major reasons for the differences. The principal fragments are intrinsically much brighter than the companions and their light curves are, to the extent known, more or less symmetrical with respect to perihelion. By comparison, the companion fragments usually exhibit a steep drop in brightness after perihelion, if they survive that long. The process of disintegration for at least two — C/1996 Q1 and C/2019 Y4 — began early and their demise may have been essentially completed by the time of perihelion or shortly afterwards.

The principal fragment always returned to perihelion first, a circumstance that has a diagnostic value as proposed below. This rule is known to also apply to the non-tidally split comets with persistent companions in the short-period orbits, e.g., 3D/Biela, 73P/Schwassmann-Wachmann, 79P/du Toit-Hartley, 141P/Machholz, etc. (see Marsden & Williams 2008).

The range of time lags of the companion fragments trailing behind the principal fragments at perihelion is astonishing, extending from as little as 0.21 yr for the pair of C/1988 F1 and C/1988 J1 to 175.5 yr for the pair of C/1844 Y1 and C/2019 Y4, nearly three orders of magnitude. Persistent companions of the split comets in short-period orbits, such as 3D, 73P, or 141P, are known to pass perihelion a few hours to about one day after the principal fragment, which is on the order of hundredths of one percent of the orbital period. On the other hand, the lag for C/2019 Y4 equaled fully 2.3 percent of the orbital period of C/1844 Y1, if not more.

When a comet in a long-period orbit splits into two fragments that survive a full revolution about the Sun, the companion fragment arrives at its perihelion at a time different from the perihelion time of the principal fragment. This differential effect could be triggered by (i) the separation velocity, (ii) the sublimation-driven nongravitational acceleration, and/or (iii) the indirect planetary perturbations (even in the absence of either fragment's close encounter with a planet).

I now investigate the magnitude of the differential effect in the orbital period for each of the three categories of provenance. I assume that the companion separates from the parent in the general proximity or perihelion. Differentiating the expression for the orbital velocity V_{orb} as a function of heliocentric distance r at a fixed location of the fragmentation event, given by r_{frag} , the relation between the separation velocity, $V_{sep}(r_{frag})$, measured along

¹ See https://minorplanetcenter.net/db_search.

Table 21
Characteristics of and Relationships Among Members of Groups of Long-Period Comets

Group	Principal fragment	Companion fragment	Perihelion distance (AU)	Perih. time (yr)	Perih. time difference ^a (yr)	Separation velocity ^b (m s ⁻¹)	Acceleration γ (units ^c)	Orbital period P_{orig} (yr)	Difference ^d ΔP_{orig} (yr)
A	C/1988 A1 (Liller)		0.841	1988.2				2932 ± 6	
		C/1996 Q1 (Tabur)	0.840	1996.8	+8.6	0.09	587	12,300 ± 1500	+9368
		C/2015 F3 (SWAN)	0.835	2015.2	+27.0	0.29	1842	3263 ± 44	+331
		C/2019 Y1 (ATLAS)	0.838	2020.2	+32.0	0.34	2183	3111 ± 2	+179
B	C/1988 F1 (Levy)		1.174	1987.9				13,960 ± 56	
		C/1988 J1 (Shoemaker-Holt)	1.174	1988.1	+0.2	≪0.01	3	13,840 ± 28	-120
C	C/1844 Y1 (Great Comet)		0.251	1844.9 _s				7600 ± 1100	
		C/2019 Y4 (ATLAS)	0.253	2020.4	+175.4 _s	0.21	4616	4844 ± 11	-2756
D	C/1847 C1 (Hind)		0.042 ₆	1847.2				8300 ± 400	
		Lick Object	1921.6	+74.4	0.03	1792
E	?		
		C/1915 R1 (Mellish)	0.465	1915.8
		C/2016 R3 (Borisov)	0.448	2016.8	2330 ± 880

Notes.

^a Difference between the perihelion time of the companion fragment minus the perihelion time of the principal fragment. The plus sign indicates that the companion arrived at its perihelion later than the principal mass. For a breakup at previous perihelion, this is the difference between the orbital periods of the two fragments, ΔP .

^b Separation velocity along the orbital velocity vector for a breakup at previous perihelion.

^c Units of 10^{-5} the solar gravitational acceleration.

^d Difference between the original orbital period of the companion fragment minus the original orbital period of the principal fragment.

the orbital-velocity vector, and the corresponding relative change in the orbital period, $\Delta P/P$, is

$$V_{\text{sep}}(r_{\text{frg}}) = \frac{k_0^2(1-e)}{3qV_{\text{orb}}(r_{\text{frg}})} \frac{\Delta P}{P}, \quad (22)$$

where q is the perihelion distance of the parent comet, e its eccentricity, and k_0 the Gaussian gravitational constant. In a pseudo-parabolic approximation,

$$V_{\text{sep}}(r_{\text{frg}}) = \kappa \sqrt{r_{\text{frg}}} P^{-\frac{5}{3}} \Delta P, \quad (23)$$

where the constant κ equals

$$\kappa = \frac{1}{3} 2^{\frac{1}{6}} \pi^{\frac{2}{3}} k_0^{\frac{1}{3}}. \quad (24)$$

When r_{frg} is given in AU, P and ΔP in years, and V_{sep} in m s⁻¹, the constant is numerically $\kappa = 7020$.

The differential effect of a nongravitational acceleration consists in the fact that the fragments orbit the Sun in gravity fields of slightly unequal magnitudes. The effect on the orbital period, P , follows from Kepler's Third Law

$$P = \frac{2\pi}{k_0} a^{\frac{3}{2}}, \quad (25)$$

where a is the semimajor axis. Differentiating this equation with respect to k_0 , which is no longer a constant, one finds

$$\Delta P = -\frac{2\pi}{k_0^2} \Delta k_0 a^{\frac{3}{2}}, \quad (26)$$

so that

$$\frac{\Delta P}{P} = -\frac{\Delta k_0}{k_0} = -\frac{\Delta k_0^2}{2k_0^2} = \frac{1}{2} 10^{-5} \gamma. \quad (27)$$

Here γ is the parameter of the nongravitational model applied in Section 3 to investigate the fragmentation of C/2019 Y4; see also Equations (10) and following. The units of γ have been 10^{-5} the solar gravitational acceleration.

Even though the planets gravitationally affect the motions of comets in all six elements, the perturbations of the reciprocal semimajor axis, $1/a$, have always been of primary interest because they present changes in the orbital energy and are relevant to the issues of comets' perihelion returns or escape from the Solar System. The indirect perturbations of $1/a$ of long-period comets were investigated extensively by Everhart & Raghavan (1970). Everhart (1968) also undertook a Monte Carlo study of perturbations by a single planet, concluding that their distribution was not Gaussian.

As two long-period fragments are on their way to aphelion, the indirect planetary perturbations essentially cease at heliocentric distances smaller than 50 AU. By that time the separation distance between the two objects has not increased enough to imply a major differential perturbation effect. However, even in the absence of a significant contribution from a separation velocity and/or a nongravitational acceleration, the aphelion distances of the fragments are not identical. It is near aphelion, where their separation distance could increase dramatically, so that the original semimajor axes of the fragments determined from their subsequent near-perihelion arcs could become clearly uneven because of the unequal integrated effects of the indirect planetary perturbations at heliocentric distances smaller than 50 AU.

Changes in the original orbital energy (i.e., its value near aphelion, referred to the barycenter of the Solar System), $\Delta(1/a)_{\text{orig}}$, are convertible into changes in the

original orbital period, P_{orig} . Since Kepler’s Third Law can obviously be written as

$$P_{\text{orig}} = \frac{2\pi}{k_b} (1/a)_{\text{orig}}^{-\frac{3}{2}}, \quad (28)$$

with k_b being the “barycentric” Gaussian constant, the differentiation with respect to $(1/a)_{\text{orig}}$ gives

$$\Delta P_{\text{orig}} = -\frac{3\pi}{k_b} a_{\text{orig}}^{\frac{5}{2}} \Delta(1/a)_{\text{orig}} \quad (29)$$

and, dividing Equation (29) by Equation (28),

$$\Delta P_{\text{orig}} = -\frac{3}{2} P_{\text{orig}} a_{\text{orig}} \Delta(1/a)_{\text{orig}} = -\frac{3}{2} P_{\text{orig}}^{\frac{5}{3}} \Delta(1/a)_{\text{orig}}, \quad (30)$$

where the expression on the right applies only when P_{orig} — and ΔP_{orig} — are reckoned in years. Instead of differentiation one can work directly with the differences.

7.2. Numerical Results for the Individual Groups

I now assess the three proposed sources for ΔP and ΔP_{orig} . For the sake of simplifying the matters, I assume that the parent comet fragmented at perihelion. The results in Table 21 offer surprisingly robust conclusions about effects of the separation velocity, the nongravitational acceleration, and the indirect planetary perturbations on the returns of the fragments to perihelion.

First of all, it is not accidental that the orbital periods of comets in the groups or pairs are not longer than thousands of years. If they were many tens of thousands of years or longer, the fragments would have been returning over periods in the past well beyond our records of cometary orbits. In fact, Table 21 illustrates that we already begin to have problems of this kind (such as the missing principal fragment of Group E). In this context, it is possible, for example, that the disintegrating comet C/1999 S4 (LINEAR) was a companion to a principal fragment whose orbital period may have been, say, 100,000 yr or so and had returned to perihelion a number of centuries earlier, as I already suggested (Sekanina 2000). C/1999 S4 masqueraded as a potential Oort Cloud comet (see footnote 1 on page 19), but was strongly deficient in carbon monoxide ice (Weaver et al. 2001), which helped reveal its true origin.

Separation velocities can hardly be the source of the investigated effect on companion fragments that are all *trailing* the principal fragments. On the contrary, one expects that effects of the separation velocity should lead to statistically equal numbers of companion fragments preceding and following the principal fragments. Even though the dataset in Table 21 is very small, the absence of leading companions is striking. Also suspect are the minuscule magnitudes of the derived separation velocities; one would have to assume that *all* fragmentation events occurred far from the Sun, thereby dramatically increasing the effect of r_{frag} in Equation (23).

Effects of the nongravitational acceleration are consistent with the dominance of trailing companion fragments, but the obvious problem is the gigantic magnitude of the acceleration required (with the exception of C/1988 J1). Objects with such enormous nongravitational effects could not appear as observable objects and survive the entire revolution about the Sun. There is also no correlation between the likelihood of survival and

the magnitude of ΔP in Table 21. For example, if the nongravitational acceleration governed this relationship, one would expect C/2019 Y1 much more likely to have begun disintegrating before perihelion than C/1996 Q1, contrary to the observed behavior of the two comets. Yet, it should be admitted that the nongravitational acceleration *does to a degree contribute* to the distribution of perihelion returns among the companion fragments, tilting ΔP to positive values in Table 21.

This leaves the indirect planetary perturbations as the major source of the effects that influence the semichaotic timing of the companion fragments’ perihelion returns. The three well-established groups/pairs in Table 21 suggest a strong dependence on the perihelion distance. One could also note that this empirical finding fits in with a pair of the Kreutz sungrazers, even though these comets have distinctly shorter orbital periods. While the perihelion returns of the companion fragments of the Liller group lagged the principal fragment, whose perihelion distance amounted to 0.84 AU, by 0.3 percent to 1.1 percent of the principal fragment’s orbital period, C/2019 Y4 trailed C/1844 Y1, whose perihelion distance was 0.3 the value of C/1988 A1, by at least 2.3 percent of its orbital period. By comparison, the Kreutz sungrazer C/1965 S1 (Ikeya-Seki), a less massive sibling of C/1882 R1 (Great September Comet), trailed the latter at perihelion by >11 percent of its orbital period.

In any event, the pair of C/1844 Y1 and C/2019 Y4 is an extreme case among the known groups/pairs of long-period comets. If the tabulated original orbital period of 7600 yr for C/1844 Y1 (Marsden et al. 1978) is replaced by T. Kobayashi’s value of 4000 yr (Green 2020a), the perihelion return of C/2019 Y4 would have lagged that of the principal fragment by as much as 4.4 percent of its orbital period, but still by significantly less than in the case of the Kreutz pair. And even though the value of ΔP_{orig} would change from -2756 yr to a positive value of $+844$ yr, the unpublished 1σ uncertainty in the orbital period of C/1844 Y1 derived by Kobayashi is estimated at hardly much less than ± 40 percent or about ± 1500 yr (given that the orbital solution had a high mean residual of $\pm 5''.2$), making ΔP_{orig} for C/2019 Y4 essentially indeterminate. Further contributing to the uncertainty is the error of P_{orig} of C/2019 Y4 itself. Because original orbital periods derived from nongravitational solutions are known to be notoriously unreliable (Marsden et al. 1973), the tabulated P_{orig} for C/2019 Y4 was taken from one of the last gravitational-orbit determinations, before introducing the nongravitational terms into the equations of motion became inevitable.

8. CONCLUSIONS

The present investigation addresses five issues associated with the genetically related pair of long-period comets, C/1844 Y1 and C/2019 Y4. The first, the Great Comet of 1844 (or 1844/1845), was a naked-eye object that burst into sight for southern-hemisphere observers a few days after perihelion in the second half of December 1844 and later was being monitored telescopically until late March 1845. The second comet was discovered about five months before perihelion and kept observers guessing about its next move. It brightened rapidly in late January 2020 only to eventually disintegrate before reaching perihelion at the end of May.

I first examine the brightness of C/2019 Y4: (i) the light curve of its nuclear condensation from the time of a pre-discovery observation (20 December 2019) to late February 2020; and (ii) its integrated brightness (both visual and CCD) between late February and late May. Intrinsically, the nuclear condensation was fading until about 22 January, when this trend was reversed and the comet began to brighten rapidly, at a rate of 0.11 mag per day. The total apparent brightness reached a broad peak in the last days of March and began to subside at a very slow rate. The light curve then essentially stabilized according to some observers or continued to decline after another minor peak according to other observers. In May the comet became a difficult object, its solar elongation dropping below 30° on the 17th.

A major part of this paper deals with the fragmentation of C/2019 Y4. The separation vectors involving the four fragments, A, B, C, and D, introduced by the MPC, are tested as a function of time, the fragment identities are examined and where needed corrected. Application of the standard model confirms that Fragment B was the principal (and presumably the most massive) fragment. The iterations of the time of separation of B and A have failed to converge, but the distribution of residuals has gradually been improving with the separation moving to earlier times. From this standpoint, the breakup in March is clearly inadmissible, but equating the time of breakup with the onset time of the nuclear-condensation's rapid brightening around 22 January offers an acceptable solution (BA₁; Table 3), besides making sense in terms of physics. Fragment A was short lived and subject to a nongravitational acceleration of about 20 units of 10^{-5} the solar gravitational acceleration relative to Fragment B.

The other two MPC-recognized fragments, C and D, are likely to have split off from Fragment A in mid-March (solutions AC₂ in Table 5 and AD₃ in Table 13, respectively). Their motions were affected by considerably higher nongravitational accelerations, in excess of 100 units of 10^{-5} the solar gravitational acceleration relative to Fragment A. They also belonged to the category of short-lived fragments and their lifespans were, as expected, much shorter than the lifespan of Fragment A.

The separation data of A and another fragment imaged with the Haleakala-Faulkes Telescope North (code F65) on 17 and 18 April could not be assigned to any of the known pairs of fragments, but could be linked with the separation from A of the fragment measured at Osservatorio del Celado (code K51) on 9 April that likewise could not be identified with any of the other fragments. These observations are proposed to refer to a new, fifth Fragment E. Based on a correlation between sizes and accelerations for the split comets, it is estimated that the pre-split nucleus of C/2019 Y4 was initially 500 meters across, Fragment A 100 meters, and Fragments C, D, an E at most 20 meters.

The relative trajectories of the five fragments projected onto the plane of the sky are briefly studied. The most intriguing is the looped trajectory of Fragment A relative to B; the angular distance between the two fragments reached a maximum of $7''.5$ on 19 March, after which time they were gradually approaching each other until 19 April, when they were merely $3''.4$ apart. From that time on, the distance began to increase again, reaching

$8''.7$ on 1 May and $17''.4$ a week later. Until early April, the only visible fragment was A, which was very active ever since the time of breakup in late January.

The third item discussed is the history of orbit determination of C/1844 Y1. The first major result was a hyperbolic orbit by Bond (1850), which was shown to be erroneous by Fayet (1910). The corrected orbit was an ellipse with an orbital period of nearly 30,000 yr, fitting the normal places only slightly better than a parabola. My orbit from 1974, based on 41 most consistent astrometric observations (a mean residual of $\pm 1''.8$) and later incorporated into Marsden et al.'s (1978) paper, yielded an original orbital period of 7600 ± 1100 yr. By contrast, T. Kobayashi's recently derived orbit (Green 2020a), based on a different set of 41 observations (a mean residual of $\pm 5''.2$), gave 4000 yr (1σ uncertainty not provided). I conclude that the orbital period of C/1844 Y1 equals several thousand years and cannot be determined more accurately because of low accuracy of the astrometric observations and short orbital arc available.

The fourth item addressed is the antitail of C/1844 Y1, displayed in January 1845 thanks to favorable projection conditions. Unfortunately, the moonlight was interfering on and around 18 January, the day of the Earth's crossing the comet's orbit. The full Moon was five days later. Useful observations of the antitail were reported from two locations, the Royal Observatory, Cape of Good Hope, and Bombay, India, both on days before the transit and in late January, long after the transit. Interestingly, one of the accounts noted that space between the antitail and main tail was filled with a diffused, irregular light, as predicted by the theory.

Limited analysis suggests that the antitail contained dust grains several tens of microns in diameter near its sunward end and much larger ones closer to the nucleus, ejected from it before perihelion. Position angle measurements of the antitail's northern border and main tail's axis suggest that the optically dominant dust ejecta left the nucleus between 5 days before perihelion and 12 days after perihelion.

The last item is examination of the genetically related pair of C/1844 Y1 and C/2019 Y4 as an extreme case among other such groups/pairs of long-period comets, including comparison with the Liller group of four kindred objects: C/1988 A1, C/1996 Q1, C/2015 F3, and C/2019 Y1. Subject to future confirmation by additional examples, each group/pair appears to be a product of a fragmentation event (or possibly events in the case of groups) about the time of previous perihelion (typically several thousand years ago). One (principal) fragment is intrinsically much brighter than the other (companion) fragments, some of which were observed failing to survive through perihelion, others fading precipitously after perihelion. The principal fragment always returns first, the companion fragment(s) following a fraction of a year to nearly two hundred years later. Of three potential trigger mechanisms proposed to explain the time lags of the trailing companions, the dominant effect is believed to be provided by the indirect planetary perturbations, with a minor but instrumental contribution from the sublimation-driven nongravitational effect. The separation velocity at breakup is suggested to be inconsequential because it could not explain the absolute prevalence of trailing companion fragments.

REFERENCES

- Aitken, R. G. 1915, *PASP*, 27, 244
 Bond, G. P. 1850, *AJ*, 1, 97
 Campbell, W. W. 1921a, *Nature*, 107, 759
 Campbell, W. W. 1921b, *PASP*, 33, 258
 Einarsson, S. 1915, *PASP*, 27, 243
 Everhart, E. 1968, *AJ*, 73, 1039
 Everhart, E., & Raghavan, N. 1970, *AJ*, 75, 258
 Fayet, G. 1910, *Ann. Obs. Paris*, 26A, 1
 Green, D. W. E. 2016, *CBET* 4321
 Green, D. W. E. 2020a, *CBET* 4712
 Green, D. W. E. 2020b, *CBET* 4708
 Green, D. W. E. 2020c, *CBET* 4744
 Green, D. W. E. 2020d, *CBET* 4751
 Hui, M.-T., & Ye, Q.-Z. 2020, *AJ*, 160, 91 (10pp)
 Knight, M., & Battams, K. 2020, *Astron. Telegram*, 13813
 Maclear, T. 1845a, *Mon. Not. Roy. Astron. Soc.*, 6, 213
 Maclear, T. 1845b, *Mon. Not. Roy. Astron. Soc.*, 6, 234
 Maclear, T. 1845c, *Mon. Not. Roy. Astron. Soc.*, 6, 252
 Marcus, J. N. 2007, *Internat. Comet Quart.*, 29, 39
 Marsden, B. G. 1972, *Catalogue of Cometary Orbits*, 1st ed.,
 Smithsonian Astrophysical Observatory, Cambridge, MA, 70pp
 Marsden, B. G. 1975, *Catalogue of Cometary Orbits*, 2nd ed.,
 Smithsonian Astrophysical Observatory, Cambridge, MA, 83pp
 Marsden, B. G., & Williams, G. V. 2008, *Catalogue of Cometary
 Orbits*, 17th ed., IAU Minor Planet Center/Central Bureau for
 Astronomical Telegrams, Cambridge, MA, 195pp
 Marsden, B. G., Sekanina, Z., & Everhart, E. 1978, *AJ*, 83, 64
 Marsden, B. G., Sekanina, Z., & Yeomans, D. K. 1973, *AJ*, 78, 211
 Minor Planet Center Staff 2020, *MPEC 2020-K131 & 2020-J16*
 Pole, W. 1845, *J. Bombay Branch Roy. Asiat. Soc.*, 2, 201
 Sekanina, Z. 1973, *IAU Circ.* 2580
 Sekanina, Z. 1974a, *Icarus*, 23, 502
 Sekanina, Z. 1974b, *Sky Telesc.*, 47, 374
 Sekanina, Z. 1976, in *Interplanetary Dust and Zodiacal Light*,
 IAU Coll. 31, ed. H. Elsässer & H. Fechtig (Berlin: Springer), 339
 Sekanina, Z. 1977, *Icarus*, 30, 574
 Sekanina, Z. 1978, *Icarus*, 33, 173
 Sekanina, Z. 1982, in *Comets*, ed. L. L. Wilkening (Tucson: Univ.
 Arizona), 251
 Sekanina, Z. 2000, *IAU Circ.* 7471
 Sekanina, Z. 2010, *Int. Comet Quart.*, 32, 45
 Sekanina, Z., & Kracht, R. 2016, *ApJ*, 823, 2 (26pp)
 Sekanina, Z., & Miller, F. D. 1976, *Icarus*, 27, 135
 Waterston, J. J. 1845, *Mon. Not. Roy. Astron. Soc.*, 6, 207
 Weaver, H. A., Sekanina, Z., Toth, I., et al. 2001, *Science*, 292, 1329
 Whipple, F. L. 1950, *ApJ*, 111, 375
 Williams, G. V. 2016, *MPEC 2016-S03*
 Ye, Q., & Zhang, Q. 2020, *Astron. Telegram*, 13620
 Ye, Q., Jewitt, D., Hui, M.-T., et al. 2021, *AJ*, 162, 70 (13pp)